David Taylor Research Center

Bethesda, MD 20084-5000

DTRC

DTRC/SHD-1373-01 December 1991

Ship Hydromechanics Department
Research and Development Report

Comparative Stress/Deflection Analyses of a Thick-Shell Composite Propeller Blade

by
Gau-Feng Lin

DTIC
SELECTE
JUN 03 1992
S D

92 6 01 093

92-14418

MAJOR DTRC TECHNICAL COMPONENTS

CODE 011 DIRECTOR OF TECHNOLOGY, PLANS AND ASSESSMENT

      12 SHIP SYSTEMS INTEGRATION DEPARTMENT

      14 SHIP ELECTROMAGNETIC SIGNATURES DEPARTMENT

      15 SHIP HYDROMECHANICS DEPARTMENT

      16 AVIATION DEPARTMENT

      17 SHIP STRUCTURES AND PROTECTION DEPARTMENT

      18 COMPUTATION, MATHEMATICS & LOGISTICS DEPARTMENT

      19 SHIP ACOUSTICS DEPARTMENT

      27 PROPULSION AND AUXILIARY SYSTEMS DEPARTMENT

      28 SHIP MATERIALS ENGINEERING DEPARTMENT

DTRC ISSUES THREE TYPES OF REPORTS:

1. **DTRC reports, a formal series,** contain information of permanent technical value. They carry a consecutive numerical identification regardless of their classification or the originating department.

2. **Departmental reports, a semiformal series,** contain information of a preliminary, temporary, or proprietary nature or of limited interest or significance. They carry a departmental alphanumerical identification.

3. **Technical memoranda, an informal series,** contain technical documentation of limited use and interest. They are primarily working papers intended for internal use. They carry an *identifying number which indicates their type* and the numerical code of the originating department. Any distribution outside DTRC must be approved by the head of the originating department on a case-by-case basis.

REPORT DOCUMENTATION PAGE

1a. REPORT SECURITY CLASSIFICATION UNCLASSIFIED	1b. RESTRICTIVE MARKINGS
2a. SECURITY CLASSIFICATION AUTHORITY	3 DISTRIBUTION/AVAILABILITY OF REPORT
2b. DECLASSIFICATION/DOWNGRADING SCHEDULE	Approved for public release; distribution is unlimited

4. PERFORMING ORGANIZATION REPORT NUMBER(S) DTRC/SHD–1373–01	5. MONITORING ORGANIZATION REPORT NUMBER(S)

6A. NAME OF PERFORMING ORGANIZATION David Taylor Research Center	6b. OFFICE SYMBOL (If applicable) Code 1544	7a. NAME OF MONITORING ORGANIZATION
6c. ADDRESS (City, State, and ZIP Code) Bethesda, MD 20084-5000		7b. ADDRESS (CITY, STATE, AND ZIP CODE)

8a. NAME OF FUNDING/SPONSORING ORGANIZATION Office of Naval Technology	6b. OFFICE SYMBOL (If applicable) ONT 233	9. PROCUREMENT INSTRUMENT IDENTIFICATION NUMBER

| 8c. ADDRESS (City, State, and ZIP code)

800 N. Quincy St., Arlington, VA 22217-5000 | 10. SOURCE OF FUNDING NUMBERS |

PROGRAM ELEMENT NO.	PROJECT NO.	TASK NO.	WORK UNIT ACCESSION NO.
0602323N	RB23C22	2	DN501143

11. TITLE (Include Security Classification)
Comparative Stress/Deflection Analyses of a Thick-Shell Composite Rotating Blade

12. PERSONAL AUTHOR(S) Gau-Feng Lin

13a. TYPE OF REPORT Final	13b. TIME COVERED FROM_____ TO_____	14. DATE OF REPORT (Year, Month, Day) 1991 December	15. PAGE COUNT 69

16. SUPPLEMENTARY NOTATION

17. COSATI CODES			18. SUBJECT TERMS (Continue on Reverse If Necessary and Identity by Block Number)
FIELD	GROUP	SUB-GROUP	Composite Finite Element Analysis
			Propeller Fiber-Reinforced Plastic

19. ABSTRACT (Continue on reverse if necessary and identify by block number)

To assist propeller designers in developing blade designs based on composite structures, an overview of composite material characteristics and available structural analysis methods was undertaken. Using detailed analyses of a thick-shell composite and a solid bronze blade, it was shown that three-dimensional finite-element analysis is useful for predicting relevant stresses and deflections. A more simplified approach was not satisfactory. To establish the feasibility of composite blades, further information about acceptable stress and deflection levels is needed.

20. DISTRIBUTION/AVAILABILITY OF ABSTRACT ☐ UNCLASSIFIED/UNLIMITED ☒ SAME AS RPT. ☐ DTIC USERS	21. ABSTRACT SECURITY CLASSIFICATION UNCLASSIFIED
22a. NAME OF RESPONSIBLE INDIVIDUAL Frank B. Peterson	22b. TELEPHONE (Include Area Code) (301) 227-1450	22c. OFFICE Code 1544

DD FORM 1473, 84 MAR

CONTENTS

CONTENTS (Continued)

FIGURES

TABLES

NOMENCLATURE

A_{ij}, B_{ij}, D_{ij}	Elements of matrices for extensional, coupling, and bending, respectively
c	Chord length
C_{ij}	Stiffness matrix components
C_p	$(P - P_a)/0.5\rho V_s^2$
D	Thruster diameter; stiffness element
E	Elastic modulus
E_1, E_2	Young's moduli of individual lamina along and normal to fibers, respectively
E_m	Modulus for matrix
f	Maximum camber
G, G_{ij}	Shear moduli
i_T	Total rake
M	Moment
N	Force
NAB	Nickel aluminum bronze
n	Number of plies; thruster rotational speed
P	Pressure
p	Thruster pitch
P_a	Ambient pressure
r	Radial station
R	Thruster radius
t	Blade thickness
V_s	Ship speed
x_c	Nondimensional distance in chordwise direction with respect to chord length
x_R	Nondimensional radial station with respect to thruster radius
z	Vertical (through-the thickness) coordinate
Z	Number of blades
δ	Elastic deflection at blade tip
Δc_p	Pressure coefficient difference (nondimensionalized on ship speed)

ε_j	Strain components
κ_f, κ_m	Volume fraction for fiber and matrix, respectively
ν_{ij}	Poisson ratios
ρ	Density, fluid density
σ_i	Stress components
θ_s	Blade skew angle, deg

ABSTRACT

To assist propeller designers in developing blade designs based on composite structures, an overview of composite material characteristics and available structural analysis methods was undertaken. Using detailed analyses of a thick-shell composite and a solid bronze blade, it was shown that three-dimensional finite-element analysis is useful for predicting relevant stresses and deflections. A more simplified approach was not satisfactory. To establish the feasibility of composite blades, further information about acceptable stress and deflection levels is needed.

ADMINISTRATIVE INFORMATION

INTRODUCTION

Composite materials are defined as the man-made products manufactured by the assembly of at least two different materials that are chemically distinct on a macroscopic scale and have a clearly recognizable interface between them.[1-2] A typical construction involves a reinforcing fiber agent embedded in a compatible matrix material such as a resin. In general, composite materials exhibit potential advantages over noncomposite materials because they can display unique mechanical properties and characteristics not possible with a single constituent. Some properties potentially useful in marine applications include high strength- and stiffness-to-weight ratios, relative ease of manufacture and, in comparison to ferrous materials, non-magnetic property.

Since the first successful application of fiber reinforced plastics (FRP) in the 1940's[3], composite materials have undergone rapid development. During the late 1960's and early 1970's advanced composites have been developed.[3] A new group of plastic laminates, which are reinforced by fibers (such as boron, graphic, or aramid-Kevlar 49) with higher strength and stiffness than fiberglass, has opened up a new, primary structural application field which the relatively low modulus fiberglass composites cannot access.

Yet, because of the intrinsic complexities of mechanical as well as thermal interaction among constituent materials, the theoretical description of composite structures has advanced much slower than practical applications. Nevertheless it was appreciated that many properties of FRP have proved to be superior to those of conventional materials. Consequently, the present work undertook a preliminary assessment of the limitations of one form of composite structure for

use in marine propeller blades. This assessment intentionally led to an examination of the ability of present structural theory to support critical design decisions involved in design of composite propellers.

The problem was approached by performing a structural evaluation of a typical marine propeller blade design, which was constructed of a hypothetical (thick-shell) composite material. This report details the theoretical analysis, hydrodynamic loading, and finite-element analysis results. The resulting stress and deflection behavior is discussed and compared to that of an isotropic metal blade using the same blade form. An additional theoretical effort was undertaken to develop a simplified method of estimating the structural behavior of a composite blade, which did not require extensive effort to generate finite-element-analysis computer input. A FORTRAN code is presented for this method. A portion of the material in this report was previously published as Reference 4.

STRUCTURAL THEORY

PROPERTIES OF A LAMINA (PLY)

The first step in analyzing a composite structure is the determination of elastic properties of the composite, either analytically or experimentally. However, laboratory testing is time consuming and costly. Thus there is a strong impetus to develop an analytical tool capable of predicting composite properties based on constituent (fiber and matrix) properties. Though in the past many equations were derived to predict the mechanical properties of composites, most of them were either scattered throughout the literature or not of simple form. Usually the rule-of-mixtures equations were used to smear the mechanical properties of fiber and the matrix into effective ply (or lamina) properties. Chamis[5] has recently developed a viable formulation for the elastic modulus of each ply, or lamina, by the use of composite micromechanics. His unified set of equations in simple form is found to be useful.

By using Chamis's equations, Nguyen and Critchfield[6] have presented an analytical capability to compute the complete set of elastic properties for fibrous composites. The following is a brief description of their procedure :

Elastic Moduli of a Lamina

From elementary elasticity, it is known that a total of twenty-one constants is needed to describe the elastic properties of an anisotropic material. For orthotropic materials a total of nine independent elastic constants will suffice. If the material of each lamina is assumed to be transversely isotropic, only five independent elastic constants are required. These elastic constants (such as E_1, E_2, G_{12}, G_{23}, v_{12}) can be derived by using constituent material properties following Chamis's method :

$$E_1 = \kappa_f E_{f1} + \kappa_m E_m$$

$$E_2 = \frac{E_m}{1 - \sqrt{\kappa_f}\,(1 - E_m/E_{f1})} = E_3$$

$$G_{12} = \frac{G_m}{1 - \sqrt{\kappa_f}\,(1 - G_m/G_{f12})} = G_{13}$$

$$G_{23} = \frac{G_m}{1 - \sqrt{\kappa_f}\,(1 - G_m/G_{f23})} \tag{1}$$

$$\nu_{12} = \kappa_f \nu_{f12} + \kappa_m \nu_m = \nu_{13}$$

$$\nu_{23} = \frac{E_2}{2\,G_{23}} - 1$$

where E_{f1}, E_{f2}, G_{f12}, G_{f23}, ν_{f12} are elastic properties for the individual fibers in various directions; E_m, G_m, ν_m are elastic properties for the matrix; and κ_f, κ_m are volume fractions of fibers and matrix. E_1 is longitudinal modulus; E_2 and E_3, transverse moduli; G_{12}, G_{13}, and G_{23}, shear moduli; ν_{12}, ν_{13}, and ν_{23} are Poisson ratios. Here, ν_{ij} = Poisson ratio for transverse strain in the j- direction (ε_j) over the strain (ε_i) by stressing in the i- direction.

Roughly speaking, the macroscopic response of the lamina in axial tension is assumed to be predominantly due to the properties of fibers, while its behavior in both transverse tension and in transverse shear will be mainly governed by the properties of the matrix.

Elastic Stiffness of a Lamina

Lamina elastic stiffnesses based on the predicted lamina moduli can be generated from the lamina stress-strain relation

$$\{\sigma_i\} = [c_{ij}]\,\{\varepsilon_j\} \quad ; i,j = 1,2,\dots,6 \tag{2}$$

where σ_i = stress components

ε_j = strain components

c_{ij} = stiffness matrix components or lamina elastic stiffnesses

For general orthotropic materials, the stiffness matrix can be constructed from the stress-strain relation. The stiffness matrix components for a layer of orthotropic material are given in Appendix A.

THIN-LAMINATE (MULTIPLE-PLY) COMPOSITES

A laminate is an assemblage of at least two laminae (thin plies) consisting of parallel fibers stacked (or layed-up) in some prescribed manner to act as an integral structural element. Conventionally the layup of a laminate is made with the ply orientation designated by the angle between the fiber direction and primary load direction (see Fig. 1).
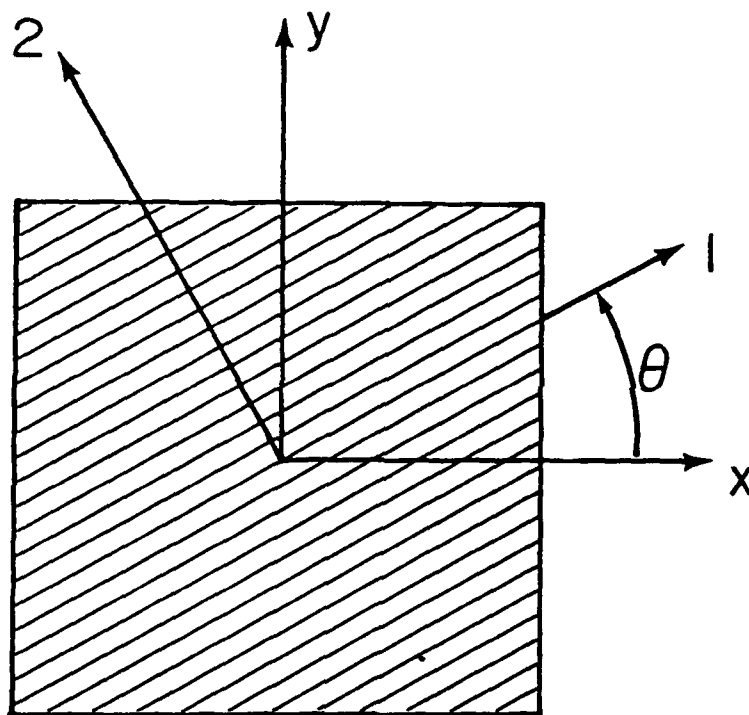
Fig 1. An off-axis unidirectional lamina.

For general laminates where the layup of laminae is not symmetric across the thickness, coupling between extension and bending will occur. When a laminate is subjected to external loading, the resulting forces and moments built up on the laminate are obtained by the integration of the stresses in each layer or lamina through the laminate thickness. The integration can be rearranged to take advantage of the fact that the stiffness matrix for a lamina is constant within the lamina, and with the substitution of the lamina stress-strain relations, one can arrive at an expression relating the resulting forces (N) and moments (M) acting

on a laminate to the middle surface strains (ε) and curvatures (κ) of the laminate by their extensional and bending stiffnesses.[6-7]

$$\left\{ \begin{matrix} N \\ M \end{matrix} \right\} = \left[\begin{matrix} A_{ij} & B_{ij} \\ B_{ij} & D_{ij} \end{matrix} \right] \left\{ \begin{matrix} \varepsilon \\ k \end{matrix} \right\} ; \quad i,j = 1,2,6 \tag{3}$$

where $\quad A_{ij} = \sum_{k=1}^{n} (\overline{Q}_{ij})_k (z_k - z_{k-1})$ $\tag{4}$

$$B_{ij} = \frac{1}{2} \sum_{k=1}^{n} (\overline{Q}_{ij})_k (z_k^2 - z_{k-1}^2) \tag{5}$$

$$D_{ij} = \frac{1}{3} \sum_{k=1}^{n} (\overline{Q}_{ij})_k (z_k^3 - z_{k-1}^3) \tag{6}$$

$$\overline{Q}_{11} = U_1 + U_2 \cos 2\theta + U_3 \cos 4\theta$$

$$\overline{Q}_{12} = U_4 - U_3 \cos 4\theta$$

$$\overline{Q}_{16} = \frac{1}{2} U_2 \sin 2\theta + U_3 \sin 4\theta$$

$$\overline{Q}_{22} = U_1 - U_2 \cos 2\theta + U_3 \cos 4\theta$$

$$\overline{Q}_{26} = \frac{1}{2} U_2 \sin 2\theta - U_3 \sin 4\theta$$

$$\overline{Q}_{66} = U_5 - U_3 \cos 4\theta$$

$$U_1 = \frac{3Q_{11} + 3Q_{22} + 2Q_{12} + 4Q_{66}}{8}$$

$$U_2 = \frac{Q_{11} - Q_{22}}{2}$$

$$U_3 = \frac{Q_{11} + Q_{22} - 2Q_{12} - 4Q_{66}}{8}$$

$$U_4 = \frac{Q_{11} + Q_{22} + 6Q_{12} - 4Q_{66}}{8}$$

$$U_5 = \frac{Q_{11} + Q_{22} - 2Q_{12} + 4Q_{66}}{8}$$

$$Q_{11} = \frac{E_1}{1 - \nu_{12}\nu_{21}}$$

$$Q_{12} = \frac{\nu_{12}E_2}{1 - \nu_{12}\nu_{21}} = \frac{\nu_{21}E_1}{1 - \nu_{12}\nu_{21}}$$

$$Q_{22} = \frac{E_2}{1 - \nu_{12}\nu_{21}}$$

$$Q_{66} = G_{12}$$

n = number of plies

Z = vertical (through-the-thickness) coordinate of each ply location (see Fig. 2)

It should be noted that the signs in the expressions of $\overline{Q}_{16}$ and $\overline{Q}_{26}$ in many publications (such as the books by Jones[1], Vinson-Chou[6], Nguyen and Critchfield's work[5], etc.) are incorrect. They should be corrected as shown above.

THICK-LAMINATE COMPOSITES

It has been often shown that classical bending theory without the effects of transverse shear deformation and rotary inertia produces errors for most thin composite laminates[8] Furthermore, transverse normal stress is neglected in the classical composite laminate theory. Pagano and Pipes[9] have demonstrated that high interlaminar normal and especially shear stresses might be responsible for onset of delamination (splitting at the interface of fiber and matrix) near the free edge of the laminate. The effect of a free edge, where highly localized stress concentrations often occur due to geometrical as well as material discontinuities, is a critical factor in the theory of laminated composites.

In view of these deficiencies, it is important not only that an adequate analytical tool be established but also that a composite be so designed as to provide through-the-thickness strength to eliminate the delamination. These requirements can only be fulfilled by a three-dimensional analysis.
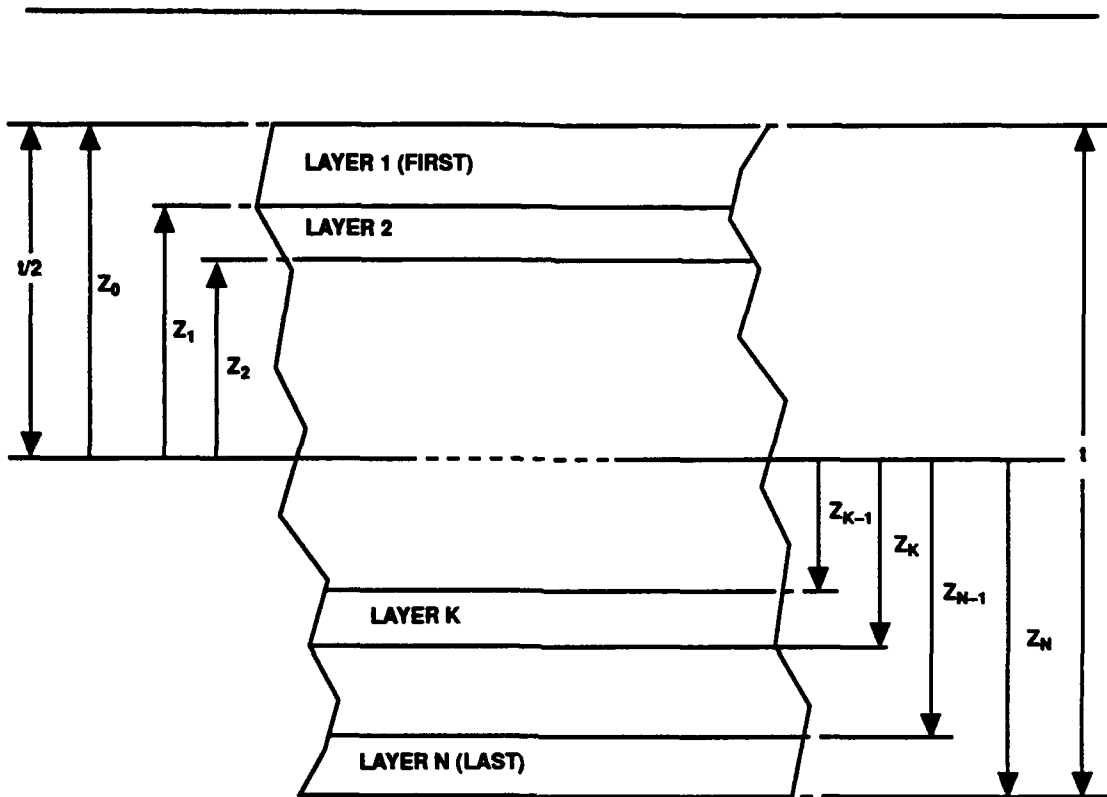
Fig. 2. *Geometry of an n-layered laminate.*

To account for 3-D features of a moderately thick laminate, Sun and Li [10] presented a procedure employing a long wave concept to derive effective elastic constants for thick laminates consisting of a repeating sublaminae. They offered two sets of expressions:

1. Full expression—this set is applied to general cases including hybrid laminates;

2. Reduced expression—this set is the simplified version of the full-expression set and is intended for a single composite system.

Theoretical predictions of the effective elastic constants for a single composite system based on the reduced expression seem to check very well with some other numerical methods and even with some limited experimental results.*

Since the full expression formulation is of lengthy form and cannot easily be understood, an alternate formulation based on the same assumptions is proposed as follows :

---

* Private communication from S. Mayes, DTRC (1990)

For a sublaminate containing N orthotropic laminae of arbitrary thickness, the effective elastic constants in the matrix $[\bar{c}]$ can be obtained :

$$\bar{c}_{ij} = \sum_{k=1}^{N} v_k \, c_{ij}^{(k)} \quad ; i, j = 1, 2, 6$$

$$\bar{c}_{33} = \frac{1}{\left(\displaystyle\sum_{k=1}^{N} \frac{v_k}{c_{22}^{(K)}} \right)}$$

$$\bar{c}_{13} = \frac{1}{2} \left[\sum_{k=1}^{N} v_k \, c_{31}^{(k)} + \bar{c}_{33} \sum_{k=1}^{N} \frac{v_k \, c_{13}^{(k)}}{c_{33}^{(k)}} \right]$$

$$\bar{c}_{23} = \frac{1}{2} \left[\sum_{k=1}^{N} v_k \, c_{32}^{(k)} + \bar{c}_{33} \sum_{k=1}^{N} \frac{v_k \, c_{23}^{(k)}}{c_{33}^{(k)}} \right]$$

$$\bar{c}_{36} = \frac{1}{2} \left[\sum_{k=1}^{N} v_k \, c_{63}^{(k)} + \bar{c}_{33} \sum_{k=1}^{N} \frac{v_k \, c_{36}^{(k)}}{c_{33}^{(k)}} \right]$$

$$\bar{c}_{pq} = \left(\sum_{k=1}^{N} \frac{v_k \, c_{pq}^{(k)}}{\Delta_k} \right) / \Delta \quad ; p, q, = 4, 5$$

$$\Delta = \left(\sum_{k=1}^{N} \frac{v_k \, c_{44}^{(k)}}{\Delta_k} \right) \left(\sum_{k=1}^{N} \frac{v_k \, c_{55}^{(k)}}{\Delta_k} \right) \left(\sum_{k=1}^{N} \frac{v_k \, c_{45}^{(k)}}{\Delta_k} \right)$$

$$\Delta_k = c_{44}^{(k)} \, c_{45}^{(k)} - (c_{45}^{(k)})^2$$

$v_k = t_k / t$ (t_k is the thickness of the kth lamina, and t is the total thickness of the sublaminate)

$c_{ij}^{(k)}$ (i, j = 1, 2, 6) : stiffness component for the kth ply ;

For a single-composite system, the above formulation reduces to that of the reduced expression given by Sun and Li[10].

WOVEN/NONWOVEN FIBER COMPOSITES

3-D textile structural composites,which are the combination of a resin system with a textile fiber, yarn or fabric system oriented in all three dimensions, have recently become important for structural applications[11]. Textile structural composite products must be made from high-modulus fibers or yarns. Yarn is an assemblage of fiber formed into a continuous strand having textile-like characteristics distributed periodically in the material. The function of the resin system is to provide rigidity and to support and protect the textile reinforcement materials (fibers, yarns, or fabrics) in a prescribed position or orientation in the composite.

The basic fabric structures can be classified[11] as

1. Wovens — made by interlacing two or more yarn systems at 90° angles;

2. Knits — made by interlooping one or two yarns;

3. Braids — made by interwining the yarn system;

4. Nonwovens — made by mechanical entanglement of fibers or by chemical bonding of the fibers at cross-over points.

The comparison of basic fabric structures is described in Table 1[11].

Because of their fully integrated nature, such as fiber continuity and 3-D fiber orientation and entanglement, the total integrated, advanced fabric systems are thought to be the most reliable for general load-bearing applications. Through-the-thickness strength and interlaminar strength for such 3-D structural composites have been greatly increased and thus the risk of splitting and delamination is minimized.

The engineering design and analysis of 3-D fabric-reinforced composites necessitates an analytical capacity that can relate the fabric geometry and processing variables to the mechanical properties of the composites. However, very little is known regarding this relationship. One typical procedure based on the concept of unit cell geometry was established by some investigators[12-16] to define the geometric parameters and their interrelationship. For example, Whyte[16] developed a Fabric Geometry Model (FGM) of unit cell by combining textile engineering methodology and a modified laminate theory to demonstrate the analysis of 3-D composites. This FGM model, specifically for 3-D braided metal matrix composite, takes into consideration the material properties, fiber architecture, and processing parameters. By using the fiber volume fraction semi-empirically introduced by Ko[12] together with the properties of the

Table 1. Comparison of basic fabric structures.

	Woven	Knitted	Braided	Nonwoven
Composition	yarn	yarn	yarn	fiber
Formation	interlace	interloop	intertwine	bond
Geometry				
Cell model				
Cell link				
Orientation	orthogonal	oblique	trellis	random
Length	short	long	short	very short
Continuity	continuous	discontinuous	continuous	either
Mobility	limited	tremendous	limited	very slight
Entanglement	flexible	mobile	flexible	rigid
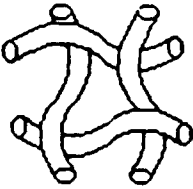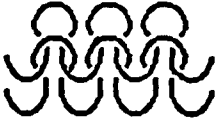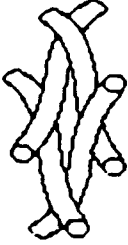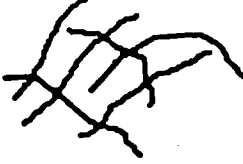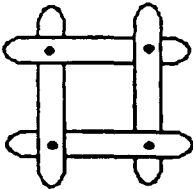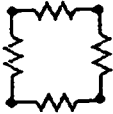
constituents, the stress-strain relation for a unidirectional composite can be established as:

$$\{\sigma\} = [c]\,\{\varepsilon\} \qquad (8)$$

The stiffness matrix $[c_i]$ for each system of yarns can be calculated by transforming the stiffness matrix $[c]$ of a unidirectional composite to the appropriate fiber orientation by the transformation matrix $[T_i]$:

$$[c_i] = [T_i]\,[c]\,[T_i]^{-1} \qquad (9)$$

The fabric-reinforced composite system stiffness is determined by superimposing proportionally the stiffness matrices from each system of yarns according to its contributing volume :

$$[c_s] = \sum k_i\,[c_i] \qquad (10)$$

where $[c_s]$ is the total stiffness matrix and k_i is the fractional volume of the ith system of yarns.

By using the stiffness matrix $[c_s]$, one can finally determine the stress-strain behavior of the fabric-reinforced composite.

The soundness of the FGM model and validity of the results for 3-D textile structural composites need further theoretical exploration and experimental verification.

FAILURE ANALYSIS

There are many different ways that failure can occur in a composite structure. For example, the possible failure modes can range from simple loss of structural stiffness due to yielding, through a premature warning of first-ply failure, interlaminar cracks, or delamination by free-edge effect, to a gross macroscopic fracture.[17,18] While failure-analysis work has been substantially performed on composite materials in the past, a general theoretically valid capability does not exist. Despite this lack, normally the determination of failure modes first requires obtaining detailed stress (strain) solutions. To achieve this, one often has to rely on the finite-element method as no other method can surpass it in its versatility. However, its determination of stress field through the assumption of a simplified displacement field in the classical laminate theory is generally not reliable. To overcome this deficiency, improved and efficient analytical tools are required. The approach by Pagano[19] and the concept by Sun and Mao[20], all referred to a global-local technique, are two such improved methods.

Assuming that composite stress analysis has been performed and that stresses and strains are available everywhere, one then can simply use the maximum stress or maximum strain theory to compare the predictive values with the allowable ones in each particular direction. However, most composite materials are known to be strongly directionally dependent. With no interaction between the material properties in different directions taken into account, a failure criterion such as maximum stress or strain may not be the best one to use when a composite is subjected to combined stresses or strains. The most commonly used failure criterion seems to be the quadratic failure criterion[21-23] in which some interaction is considered :

$$F_{xx}\, \sigma_x^2 + 2\, F_{xy}\, \sigma_x\, \sigma_y + F_{yy}\, \sigma_y^2 + F_{ss}\, \sigma_s^2 + F_x\, \sigma_x + F_y\, \sigma_y = 1 \qquad (11)$$

where $\quad \sigma_x, \sigma_y$ = normal stress in the x, y directions respectively

$\qquad \sigma_s$ = on-axis shear stress

$\qquad F_{xx}\ = \dfrac{1}{XX'}$

$$F_{yy} = \frac{1}{YY'}$$

$$F_x = \frac{1}{X} - \frac{1}{X'}$$

$$F_y = \frac{1}{Y} - \frac{1}{Y'}$$

$$F_{ss} = \frac{1}{S^2}$$

X (Y) = longitudinal (transverse) tensile strength in the x (y) direction;

X' (Y') = longitudinal (transverse) compressive strength in the x (y) direction;

S = longitudinal shear strength.

F_{xy} is taken to be $(-1/2)$[23] following the assumption that the failure criterion is a generalization of the Von Mises criterion. In general, equation (11) should be modified or transformed when directions of applied stresses do not coincide with the material axes.

By first determining the maximum length of the strain vectors which satisfies the three-dimensional ellipsoidal strain space described by failure criterion equation (11), and then comparing this with the lengths of strain vectors throughout the composite, Daoust and Hoa[23] are able to determine the safety factor in composite laminates in a noniterative fashion. This procedure and some other theories such as the Tsai-Wu theory[21], are all practical methods for predicting composite strength since test data for combined biaxial and shear strength are usually difficult and expensive to obtain.

SAMPLE ANALYSIS OF A PARTIAL-COMPOSITE BLADE

BLADE GEOMETRY

In order to estimate the usefulness of available theory for analyzing propeller blade structures, the stress and deflection characteristics of a hypothetical blade were predicted. The general arrangement of the blade configuration is shown in Fig. 3; geometric characteristics are listed in Table 2. The blade was made of a mixture of isotropic and composite materials distributed in the following distinct zones :

The tip zone: Type-4 nickel-aluminum bronze (NAB) was used in the blade tip area from $x_R = 0.8$ to the very tip end;
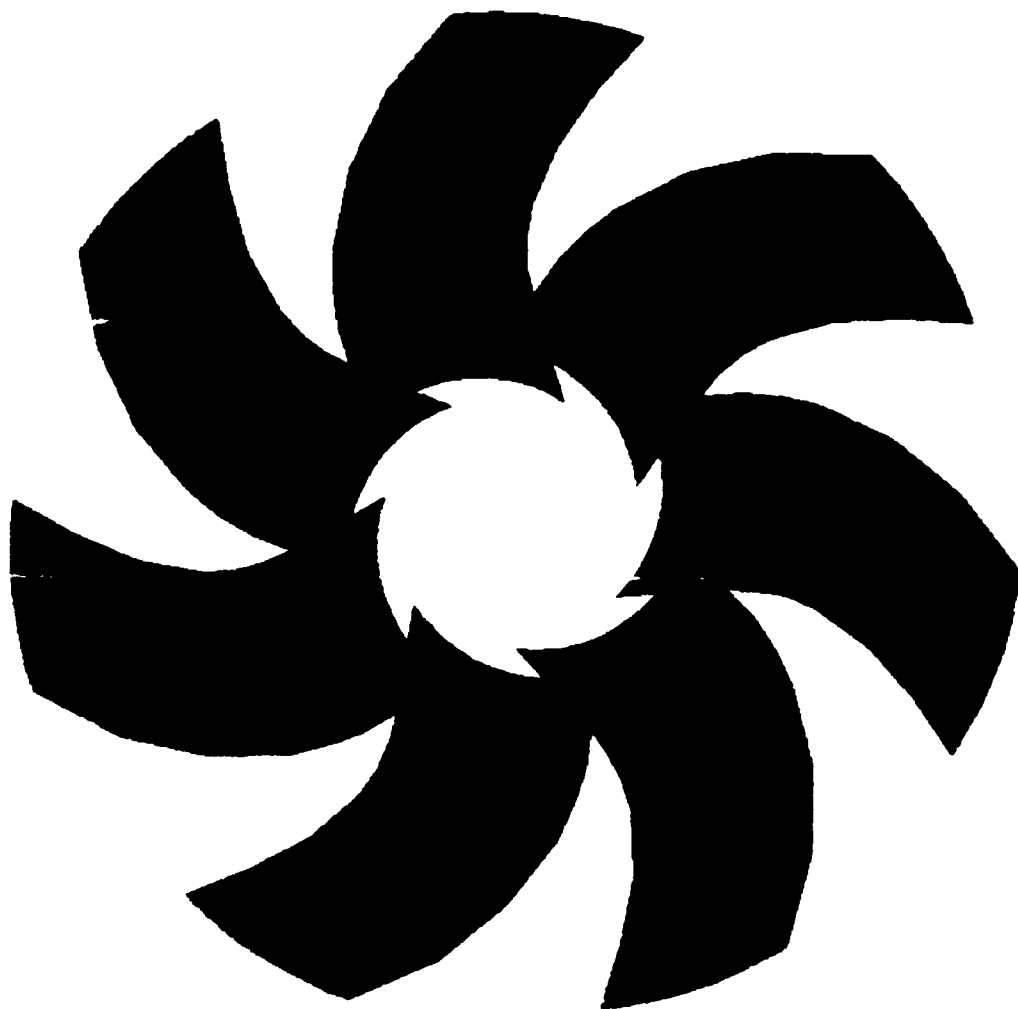
Fig. 3a General arrangement.

Fig. 3. Geometry of a seven-bladed thruster.
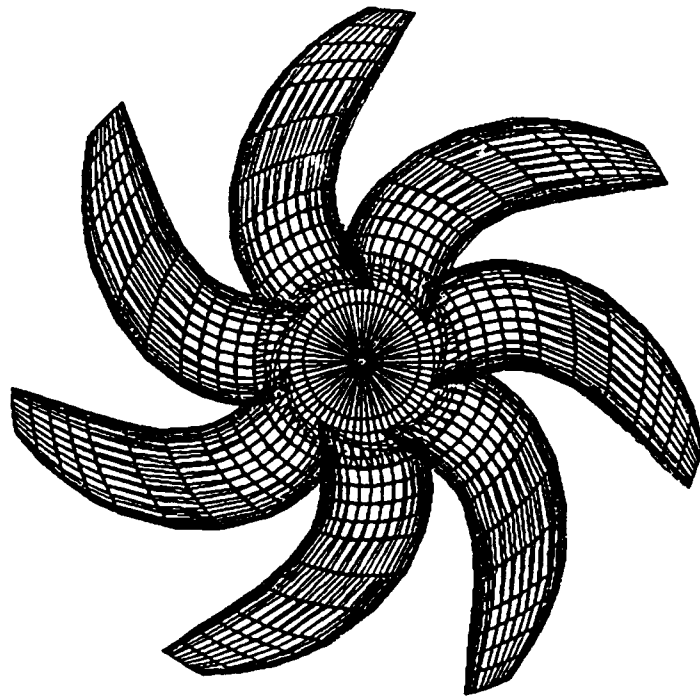
Fig. 3b. Front view.
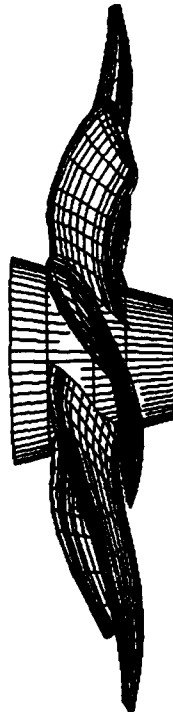
Fig. 3c Side view.

Fig. 3. Geometry of a seven-bladed thruster.

Table 2. Geometric characteristics of a composite thruster.

(a) Basic Blade Geometric parameters

Number of blade (Z)   7
Diameter (D),   21.026 cm (8.2779 in)
Skew, deg   30
Hub-diameter ratio   0.231

r/R	c/D	p/D	θs (deg.)	tT/D	t/c	f/c
.231	.1718	.5050	-3.805	-.0053	.2138	-.0243
.3	.1770	.5561	-7.402	-.0114	.1988	-.0062
.4	.1830	.7267	-6.750	-.0136	.1772	.014
.5	.1863	.8857	-2.458	-.0061	.1546	.0285
.6	.1862	.9345	3.551	.00922	.1335	.0333
.7	.1810	.8966	10.152	.0253	.1143	.0317
.8	.1651	.7849	16.792	.0366	.0995	.0242
.9	.1299	.6367	23.399	.0414	.0933	.0069
1.0	.0695	.0454	29.998	.0378	.1075	-.0488

(b) Blade Surface Form

r/R	side	Blade Surface Offsets (in) x_c					
		.0	.2	.4	6	.8	1.
.231	s	.00	.0960	.1152	.1150	.0875	.0134
	p	.00	-.1403	-.1815	-.1813	-.1317	-.0134
.3	s	.00	.1075	.1335	.1333	.0988	.0116
	p	.00	-.1189	-.1507	-.1501	-.1103	-.0116
.4	s	.00	.1182	.1517	.1515	.1100	.0099
	p	.00	-.0905	-.1101	-.1099	-.0823	-.0099
.5	s	.00	.1205	.1581	.1579	.1133	.0088
	p	.00	-.0648	-.0746	-.0744	-.0576	-.0088
.6	s	.00	.1128	.1496	.1495	.1067	.0083
	p	.00	-.0471	-.0511	-.0510	-0.411	-.0083
.7	s	.00	.0970	.1291	.1290	.0922	.00£)
	p	.00	-.0362	-.0379	-.0378	-.0315	-.0080
.8	s	.00	.0740	.0981	.0980	.0707	.0076
	p	.00	-.0317	-.0346	-.0346	-.0284	-.0076
.9	s	.00	.0438	.0561	.0561	.0418	.0073
	p	.00	-.0342	-.0418	-.0418	-.0322	-.0073
1.0	s	.00	.0061	.0032	.0033	.0051	.0055
	p	.00	-.0420	-.0571	-.0572	-.0411	-.0055

Note: (i) s is the offset from nose-tail line to suction side;

p is the offset from nose-tail line to pressure side.

(ii) To convert (in) to (cm), the values are divided by 0.3937.

The composite material zone: From the hub to $x_R = 0.8$, a cross-section of this zone reveals a sandwich configuration in which the outer thick-shell skin and the internal shear-web support were made of fiber-reinforced composites. The core is filled with anisotropic foam-type material . A combined total of approximately 20 percent of the chord length is formed of low-modulus materials streamlined for hydrodynamic purposes at leading and trailing edges.

The material properties used in the different zones are shown in Table 3. Finite element grid lines for both zones at the isotropic-composite juncture ($x_R = 0.8$) are shown in Fig. 4.

There are two important phases in dealing with the 3D geometries of a complex composite blade. First, the interior boundary between skin and core is mathematically defined and 3D solid elements for a thick-shell blade are generated. Such meshing of solids requires the accurate representation of the actual blade, fulfillment of mesh continuity, and the selection of well-shaped elements. Second, the spatial variation or orientation of material properties should be determined to define the local axis system for material definition.

COMPOSITE MATERIAL CHARACTERISTICS

The analysis of a composite structure, in contrast to that of a conventional single-material structure, is such that elastic material constants need to be determined for the composite system embedded in the structure. The analysis of laminated composites is well understood and can be readily used. However, it has been shown in classical composite laminate theory that the onset of delamination often occurs near the free edge of a laminate, where highly localized stresses concentrate due to geometric and material discontinuities. This free-edge effect can be minimized or practically eliminated by using 2-D or 3-D textile structural composites.

A particular advantage further provided by 3-D braided composites is greatly increased through-the-thickness or interlaminar strength, reducing the risk of delamination [14]. Nonetheless, 3-D composites are very expensive and the determination of their corresponding elastic constants is difficult and still state-of-the-art.

In the present study, two-dimensional braiding fabric was chosen as the composite material. Braiding fabric can be readily automated and manufactured to conform to complex shapes without free-edge effects.[24] For predicting elastic constants, the thick-laminate technique[9] was adopted to account for 3-D features, along with the assumption that composite materials are layers of orthotropic materials. It was further assumed that the skin composite layer and shear-web, consisting of large numbers of a repeating sublaminate, could be modelled as a three-dimensional homogeneous anisotropic solid. Effective moduli were derived by properly integrating the constituent lamina properties

Table 3. Material properties of a composite blade.

Material	Area	Elastic Moduli (msi) and Poisson Ratios (υ)								
		E_{11}	E_{22}	E_{33}	G_{23}	G_{13}	G_{12}	υ_{12}	υ_{13}	υ_{23}
composite	skin	5.7	1.4	1.4	0.6	0.6	0.36	0.25	0.25	0.30
	web	same	as	above						
	core	.04	.04	.04	.06	.06	.016	.25	.25	.25
isotropic	tip-zone	$E = 18$	$\upsilon = .3$	$\rho = 0.275$ lb/in^3						
	edge	$E = .01$	$\upsilon = .45$	$\rho = 0.037$ lb/in^3						

Note : (i) Fiber orientation for skin (0/60/-60 degrees);

fiber orientation for shear-web (45/-45 degrees).

Density (ρ) for composite :

0.073 lb/in^3 (skin and web) , 0.020 lb/in^3 (core).

(ii) To convert (msi) to (N/m^2), the values are multiplied by 0.006894

(iii) To convert (lb/in^3) to (kg/m^3), the values are multiplied
by 0.00927.
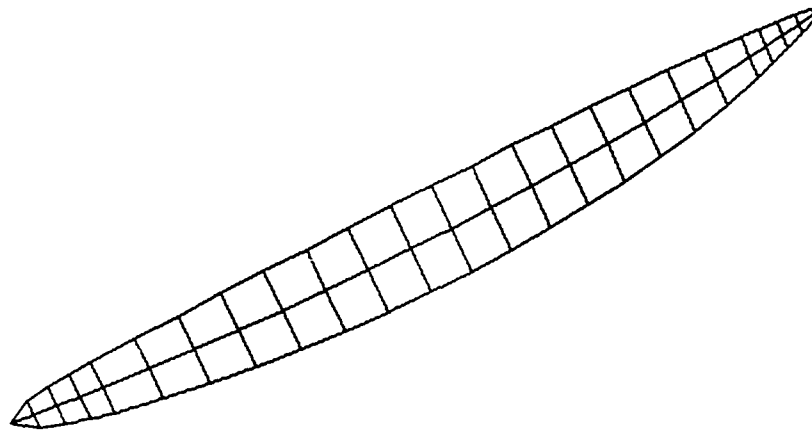
**Fig. 4a.** Tip isotropic cross section at $x_R = 0.8$.
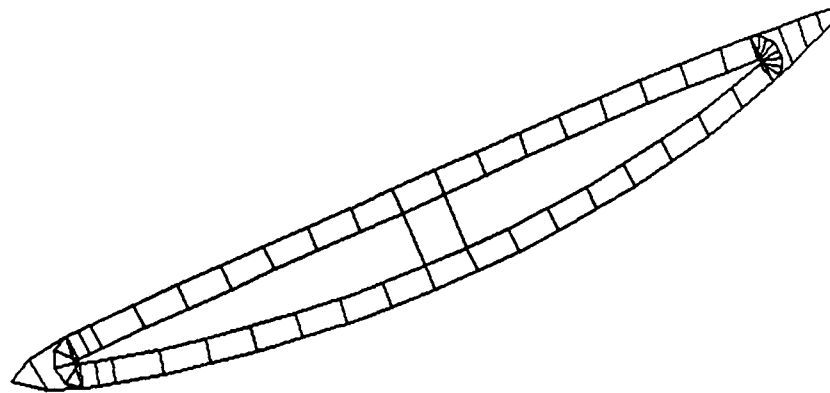
Fig. 4b. Composite cross section at $x_R = 0.8$.

Fig. 4. Cross sections of finite element model.

through the thickness of the sublaminate. Three different kinds of composite materials, as shown in Fig. 5 and Table 3, were used in the study :

1. *Monolithic triaxial E-glass spar:* This material is used in the skin layer of the composite zone. The E-glass fibers were oriented at three different angles (0,+60,-60 degrees) to the element axis and were woven continuously around the mandrel. The zero angle stands for the direction of unidirectional fibers running parallel to the braid axis. Unlike the traditional laminate stack-up, this special triaxial shell spar not only eliminates the free-edge effect but also is suitable for taking up the major bending loads produced by the hydrodynamic pressure.

2. *±45° braided E-glass:* This material was used in the shear-web of the composite zone. The E-glass fibers were oriented at ±45° to the element axis. This ±45° orientation is designed to resist the shear loads. The shear-web also increased the structural stability against buckling.

3. *Polyurethane core:* This material was used in the core area of the sandwich composite zone. The core material can not only resist the shear stress produced by the external forces but also has the important function of absorbing the energy of impacts.

Assuming orthotropic elastic symmetry for the composite materials, only nine independent elastic constants for each of the different composite materials required for the 3-D finite element analysis were calculated and tabulated in Table 4. The material orientation for a typical composite section is illustrated in Fig. 6.

BLADE LOADING

Two kinds of blade loads were considered in this analysis: hydrodynamic and centrifugal. Centrifugal load or force could be easily calculated since it is a function only of blade material density, blade rotational speed, and blade geometry. Hydrodynamic force is more difficult to predict. There are several available prediction codes. The PSF-2 numerical code was used in the present study to predict the pressure distribution. The predicted pressure coefficient difference generated at a hypothetical design ship speed of 20 knots (10.29 m/s) and a shaft revolution rate of $n = 4195$ rpm, applied on the pressure side of the blade, is plotted in Fig. 7 and tabulated in Table 5.
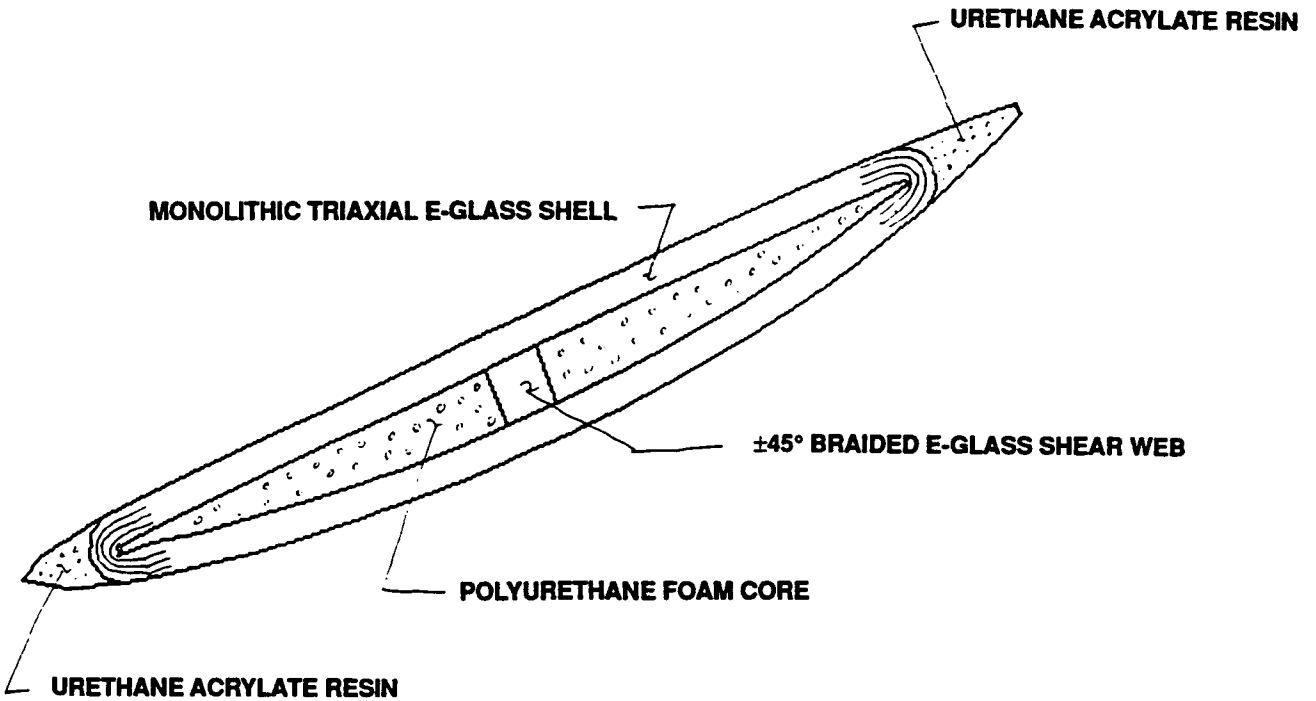
Fig. 5. Material arrangement in composite zone.

Table 4. Elastic constants of composite blade for finite-element analysis.

		Elastic Constants (msi)				for Finite -Element Analysis			
	Area	D_{1111}	D_{1122}	D_{2222}	D_{1133}	D_{2233}	D_{3333}	D_{1212}	D_{1313}	D_{2323}
composite	skin	3.26	1.04	3.26	0.515	0.515	1.58	1.11	0.45	0.45
	web	2.75	1.55	2.75	0.515	0.515	1.58	1.62	0.45	0.45
	core	.048	.016	.048	.016	.016	.048	.016	.06	.06

Note : (i) For the definitions of stiffness element D_{1111} etc, one is referred to the
ABAQUS manual.

(ii) To convert (msi) to (N/m^2), the values are multiplied by 0.006894.
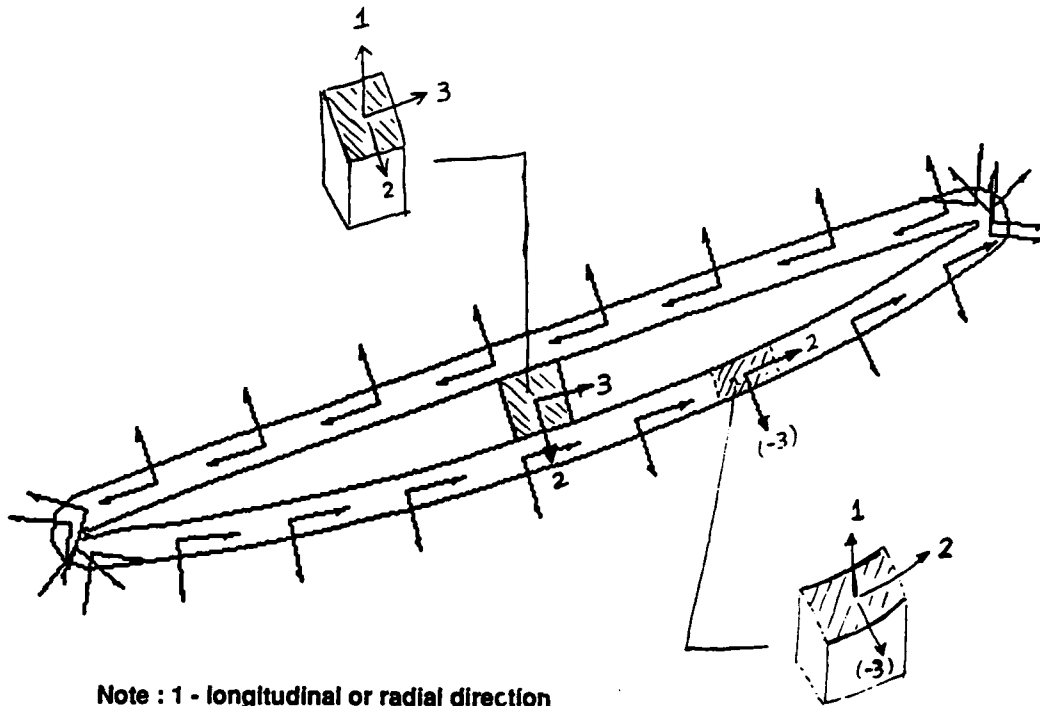
Note : 1 - longitudinal or radial direction

2 - transverse direction

3 - through-the-thickness direction

Fig. 6. Orientation for material definitions.
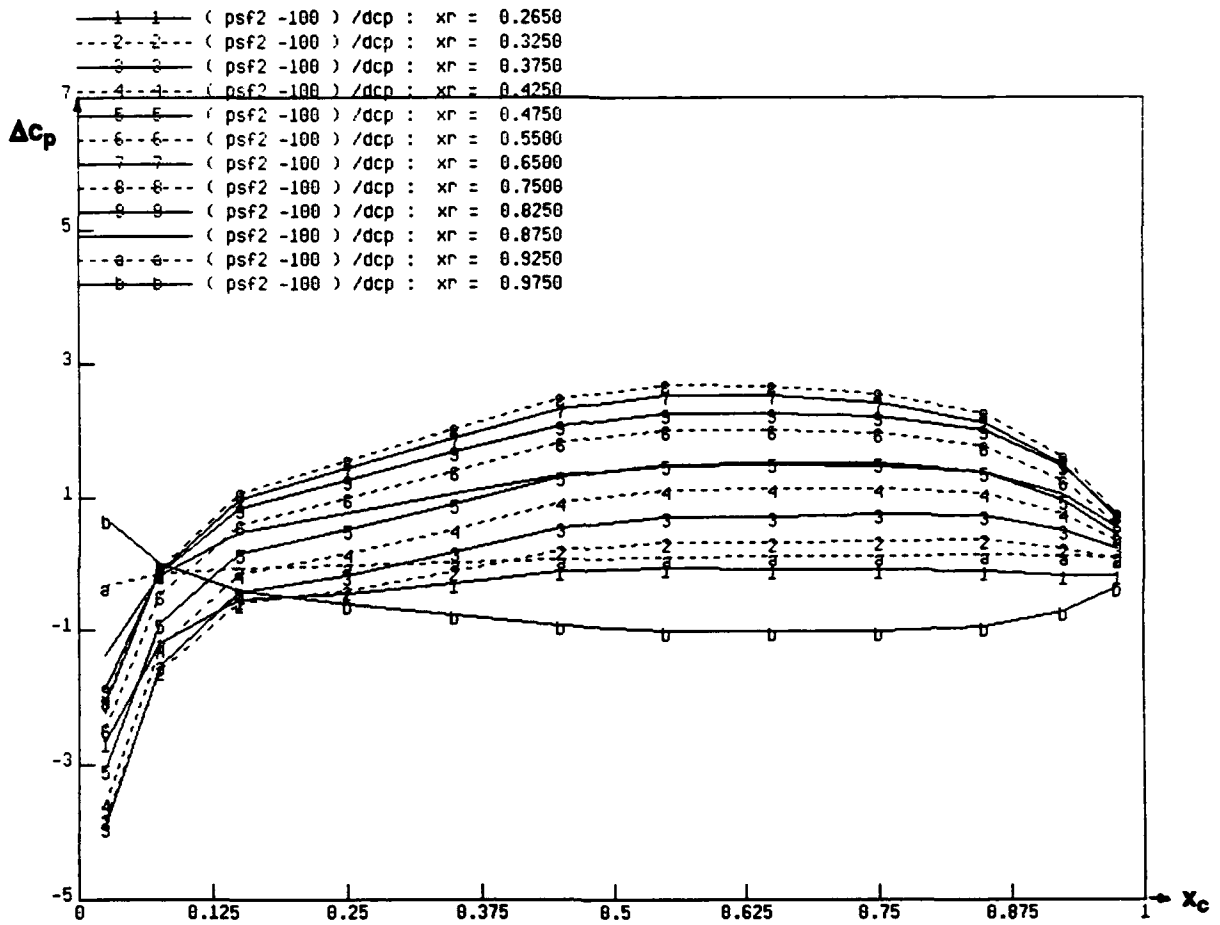
Fig. 7. Pressure difference (Δc_p) versus chordwise station (x_c)
for different stations (psf-2 code).

Table 5. Pressure difference on composite blade.

| | Pressure Difference Δc_p | | | | | | | | |
| | | | | x_c | | | | | |
r/R	.025	.25	.35	.45	.55	.65	.75	.85	.975
.265	-2.675	-.451	-.287	-.108	-.062	-.099	-.104	-.109	-.194
.325	-3.825	-.402	-.118	.199	.319	.308	.338	.358	.068
.375	-3.934	-.176	.167	.542	.700	.705	.736	.725	.217
.425	-3.584	.148	.525	.924	1.104	1.117	1.131	1.064	.331
.475	-3.066	.506	.903	1.307	1.495	1.511	1.499	1.369	.431
.550	-2.472	.985	1.404	1.812	2.006	2.014	1.961	1.750	.584
.650	-2.091	1.442	1.896	2.322	2.522	2.512	2.411	2.118	.674
.750	-2.062	1.561	2.037	2.476	2,677	2.660	2.553	2.262	.734
.825	-1.873	1.261	1.680	2.068	2.252	2.255	2.197	1.999	.727
.875	-1.369	.768	1.058	1.330	1.463	1.478	1.463	1.361	.546
.925	-.349	-.035	.014	.062	.089	.102	.117	.128	.095
.975	.684	-.607	-.778	-.935	-1.013	-1.021	-1.011	-.947	-.365

FINITE-ELEMENT STRESS ANALYSIS

### ABACUS Computer Code

From the geometric input and the material orientation at the centroid of each solid element in the composite zone, the finite element code ABAQUS[25] was used to perform the stress analysis. The ABAQUS code is a general purpose finite-element computer code for production use in a wide range of applications. It has an extensive library of nonlinear features. Input is organized in key words and sets. The ABAQUS code has been successfully applied in many engineering problems. For example, the tip motion of a geometrically nonlinear isotropic cantilever beam with a circular pipe cross-section was obtained by using ABAQUS (see example 1.2.1 in Ref. 24) and compared excellently with the exact solution for the inextensive beam[26]. An anisotropic composite plate was analyzed by using ABAQUS(see example 4.4.1 in Ref. 25) and yielded deflection and moment values which compared closely with the analytical solution.[27]

Two different kinds of elements were used in the blade: 20-node and 15-node curved solid elements. They were adopted to represent the curve- and skew-geometry of the entire blade. There were a total of 430 solid elements. Except for six 15-node triangular prisms used in the high curvature leading edge of the composite zone, the remaining are 20-node elements. The boundary condition required that nodal points on the intersection of blade and hub be held fixed. Care was taken along the $x_R = 0.8$ section, the dividing juncture between isotropic and composite zones, that MPC (multi-point constraints) were properly employed to ensure structural connectivity.

Failure Criterion

No failure criterion tailored especially for composite materials was employed for this analysis. Instead, to simplify the analysis, stresses were considered to exceed allowable levels when the elastic limit of the material was exceeded. For this purpose the effective stresses were obtained from the effective modulus model of Sun and Li.[10] (In a more general treatment, failure criteria would be applied to individual through-the-skin stress levels recovered from effective stresses computed by the global-local technique[28].)

Numerical Results

Numerical results were obtained for the blade with a partial composite-shell structure, and, for comparison, a second blade of solid NAB, which, of course, is isotropic. The same geometry and loading were used in both cases.

Calculated elastic deflections for both the composite and isotropic blades are shown in Figs. 8 and 9. As can be seen, the deflection pattern of the composite blade is similar to that of the isotropic blade. However, the maximum deflection at the tip of the composite blade, listed in Table 6, is an order of magnitude larger than that of the isotropic blade. This relatively large deflection has the potential of causing a significant change in geometric shape.

Calculated stresses in the radial direction on the suction and pressure sides for the composite blade (excluding the isotropic tip zone) are plotted in Figs. 10 and 11. The principal stresses for the isotropic blade are plotted in Figs. 12 and 13. These principal stress values are predominantly in the radial direction, and therefore correspond closely to radial stress values. Shear stresses on the pressure side for composite and isotropic blades are plotted in Figs. 14 and 15, respectively. Through-the-thickness tensile stress for the composite blade is plotted in Fig 16.

By comparing Fig. 10 with Fig. 12, it is seen that the stress contours on the suction side for both composite and isotropic blades exhibit a similar trend, in that the maximum stress is located near the mid-chord of the blade-hub intersection, with smaller stress magnitudes toward the tip and leading edge. Similarly, Figs. 11 and 13 show that stress contours on the pressure side also exhibit a similar pattern for both composite and isotropic blades, with the maximum stress occurring near the trailing edge (0.85 chord-length measured from leading edge) around the radial station x_R=0.35. Maximum shear stresses (Figs. 14 and 15) also occur close to the trailing edge near the root

A more detailed examination was made of the through-the-thickness tensile stress distribution. The maximum through-the-thickness tensile stress is seen from Fig. 16 to occur on the inner surface of the thick-shell skin layer at the trailing edge near the root. The stress distribution in the thickness direction was

Table 6. Maximum stress and deflection values.

Response		NAB Blade **		Composite Blade**	
		FEA	Simple Beam	FEA	Simplified Method
Stress* (psi)	S_{11} ss	-5060	-5900	-8350	-7060
	S_{11} ps	5916	7130	8050	7490
	S_{12}	2280	2250	3067	1528
	S_{33}	—	—	2600	—
Deflection (in.)	δ	0.0073	—	0.072	0.052

* S_{11} : Bending stress in the radial direction (for simple beam this is referred to principal stress;

S_{12} : Shear stress on the blade cross-section in the skin layer parallel to the blade surface;

S_{33} : Through-the-thickness tensile stress in the skin layer thickness direction;

(+) Tensile stress; (-) Compressive stress;

ss : suction side; ps : pressure side; δ : elastic deflection at blade tip.

** The working stress levels of NAB are taken to be approximately[29]

S_{11} (tension) = 9000 psi; S_{11} (compression) = -9000 psi;

S_{12} = 4500 psi. For composite triaxial E-glass material, ultimate strength stress values were estimated by the quadratic failure criterion[21] to be:

S_{11} (tension) = 8100 psi; S_{11} (compression) = -35600 psi;

S_{12} = 6300 psi. For S_{33}, matrix ultimate strength is expected to be about 3000 psi.

Note: To convert (psi) to (N/m^2), the values are multiplied by 6894; to convert (in.) to (cm), the values are divided by 0.3937.
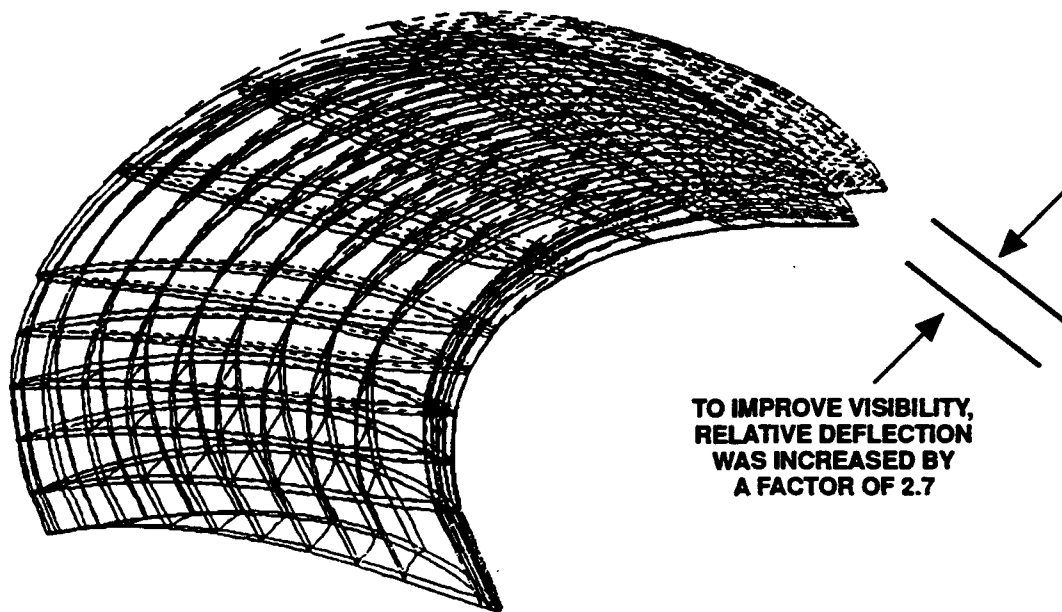
Fig. 8. Deflection of composite blade.
(Solid line: displaced mesh; dashed lines: original mesh).
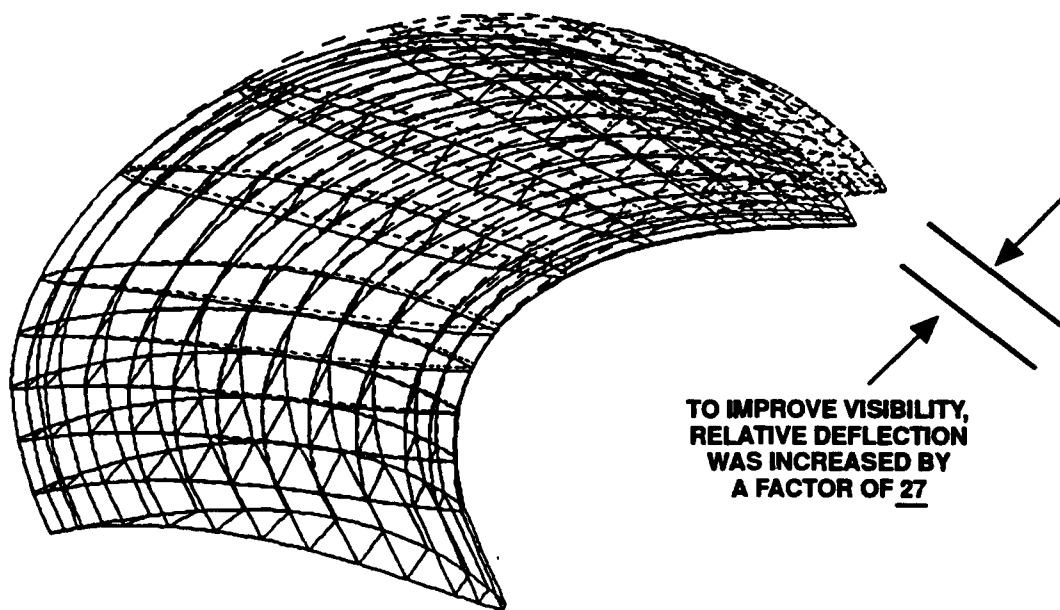
Fig. 9 Deflection of solid NAB blade.
(Solid line: displaced mesh; dashed lines: original mesh).
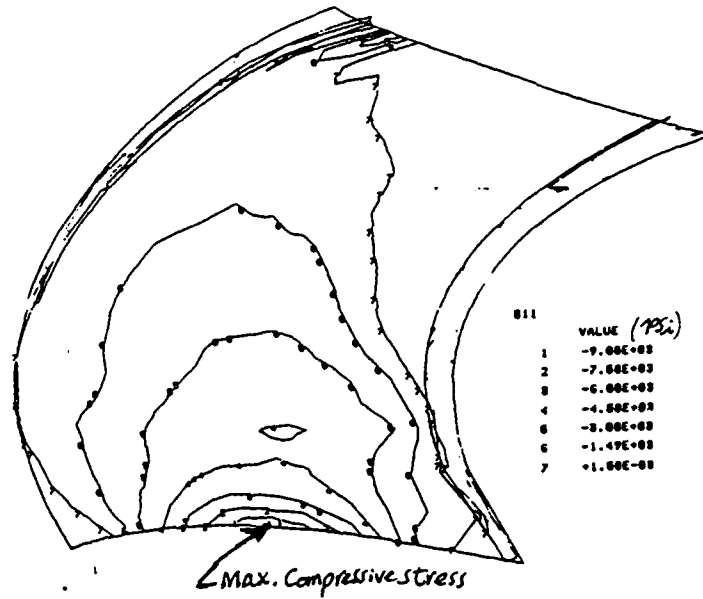
Fig. 10. Compressive radial stress contour on suction side (composite blade).
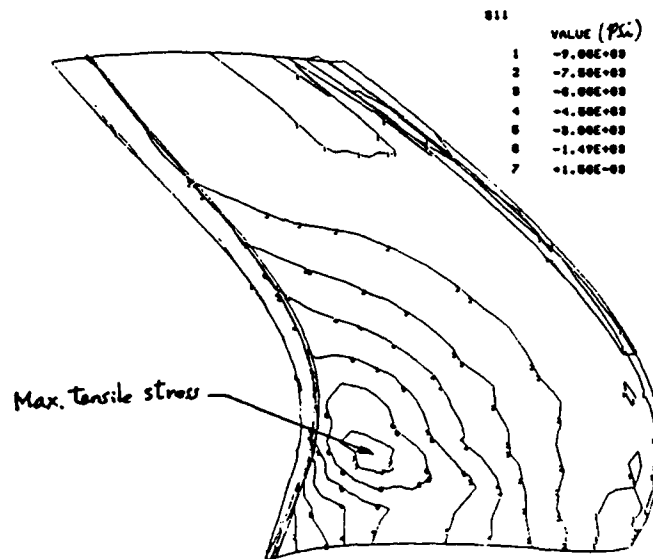
Fig. 11. Tensile radial stress contour on pressure side (composite blade).
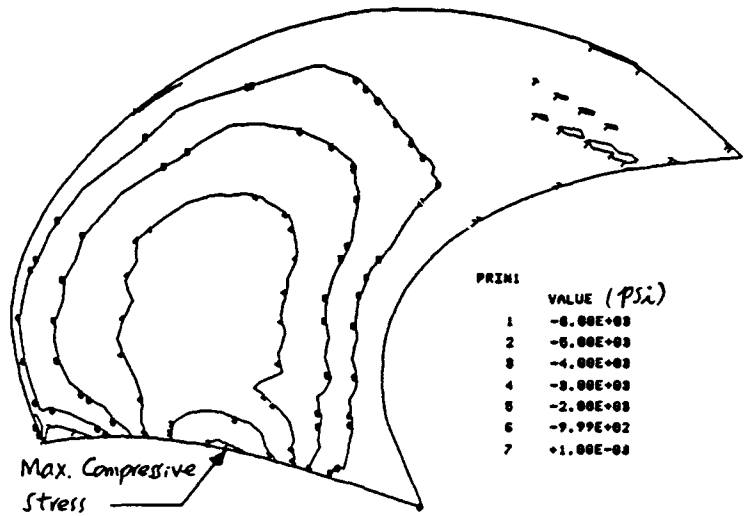
Fig. 12. Principal (compressive stress contour on suction side (solid blade).
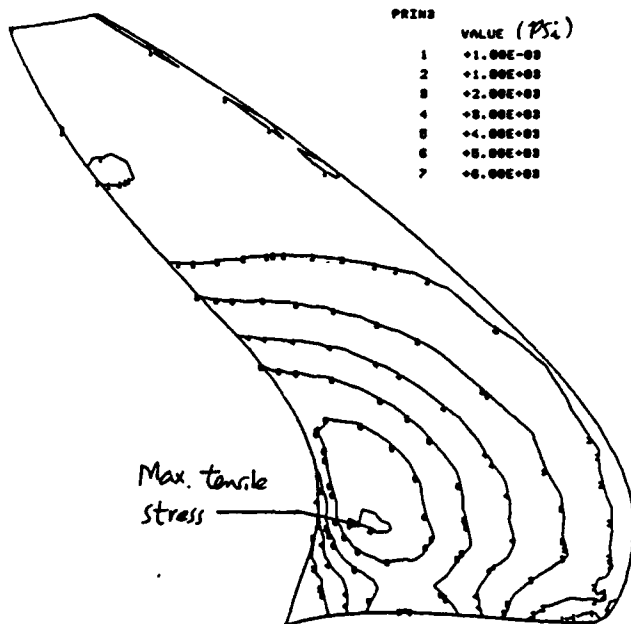
Fig. 13. Principal (tensile) stress contour on pressure side (solid blade).
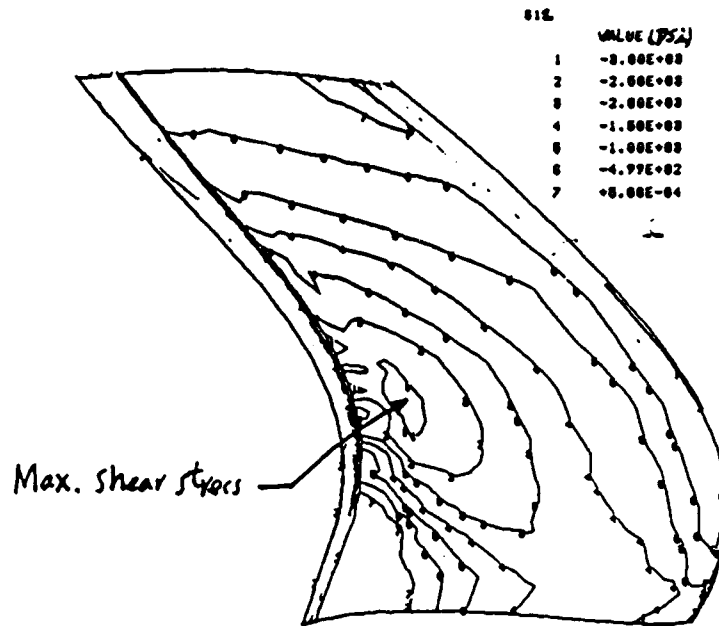
Max. Shear stress

Fig. 14. Shear stress contour on pressure side (composite blade).

Max. Shear stress

Fig. 15. Shear stress contour on pressure side (solid blade).

S33

VALUE *(psi)*

1	+2.00E-04
2	+2.00E+02
3	+4.00E+02
4	+6.00E+02
5	+8.00E+02
6	+1.00E+03
7	+1.20E+03

Max. S_{33}

A — A
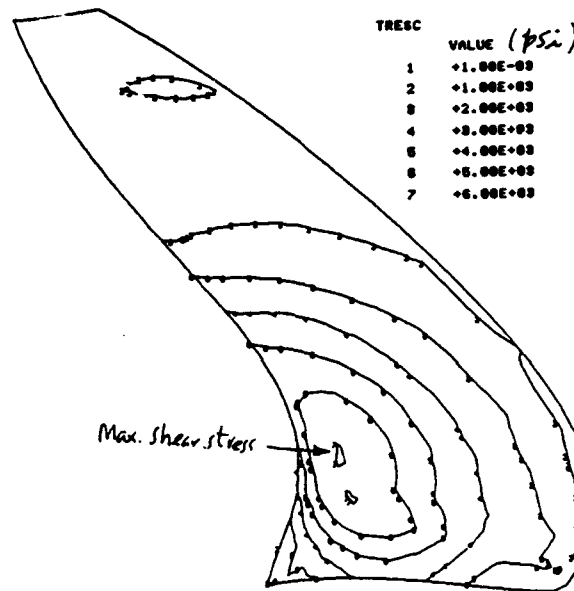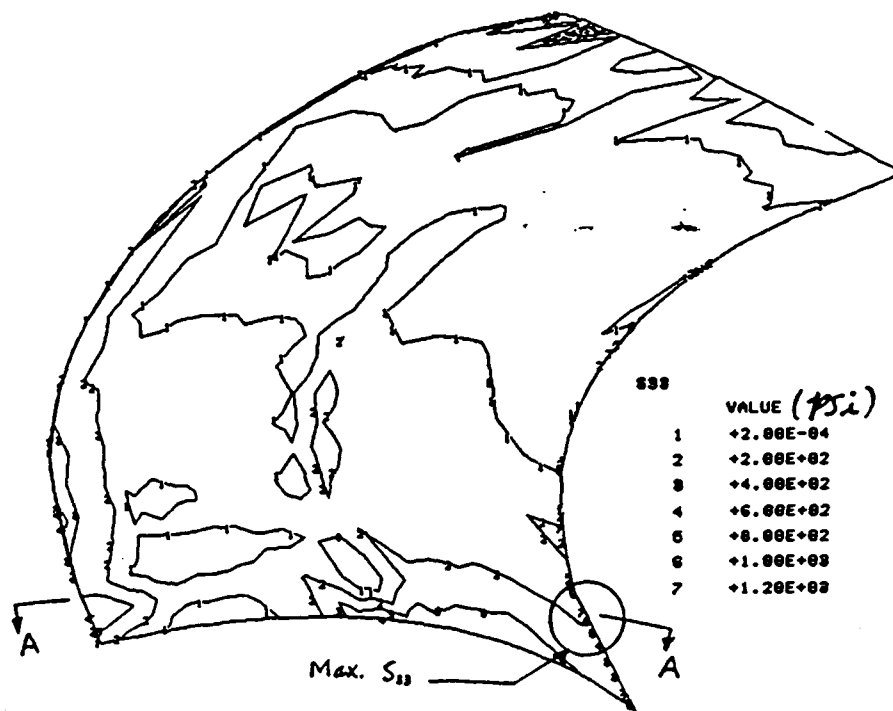
Fig. 16a. Blade planform.

Fig. 16. Contours of through-the-thickness tensile stress on the pressure side of composite blade.

S33

VALUE *(PSi)*

1 +2.00E-04
2 +2.00E+02
3 +4.00E+02
4 +6.00E+02
5 +8.00E+02
6 +1.00E+03
7 +1.20E+03

Detail B
(Max. S_{33})

TE

LE
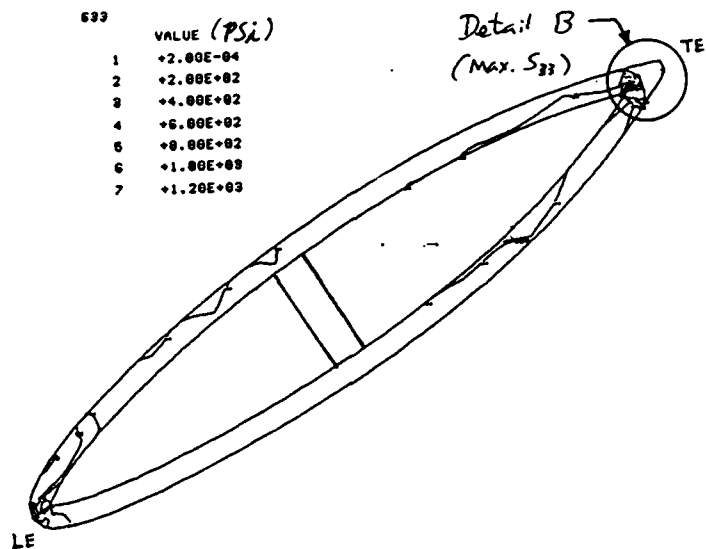
Fig. 16b. Blade cross section A-A at $x_R = 0.3$.

Skin layer Boundary

TE
(isotropic)

(Composite)

Max. S_{33}

S33

VALUE *(PSi)*

1 +2.00E-04
2 +2.00E+02
3 +4.00E+02
4 +6.00E+02
5 +8.00E+02
6 +1.00E+03
7 +1.20E+03
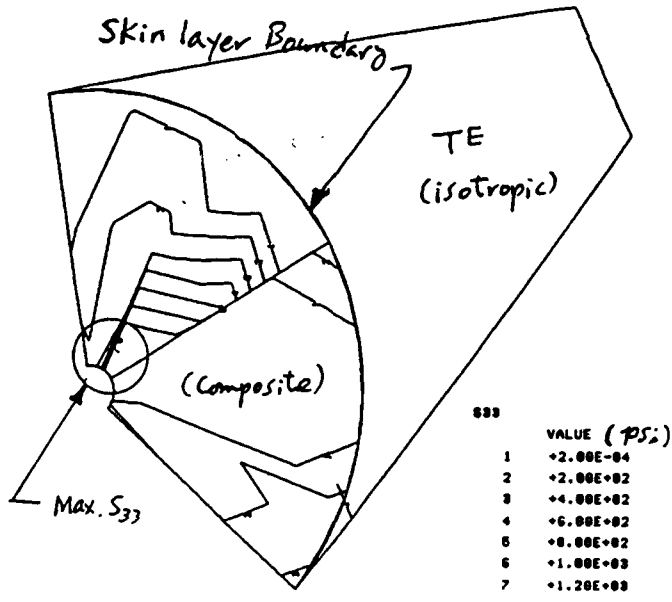
Fig. 16c. Blade cross section (Detail B at $x_R = 0.3$).

Fig. 16. (Continued)

such that the maximum tensile stress generated on the inner shell surface decreased to a smaller stress level toward the outer skin layer.

The maximum stresses and deflections for both NAB and composite blades are summarized in Table 6, along with NAB blade stress values calculated by a simple beam theory customarily used for propeller design work. For NAB, the maximum stresses predicted by FEA did not exceed 66 percent of the allowable working levels as indicated in the table notes. Beam theory consistently gave higher values, up to 79 percent of the allowable levels. Both results imply that the NAB blade design would be adequate for operation at higher than the hypothetical design speed.

The composite stresses were compared against estimated ultimate strength levels. The in-plane predicted stresses reached over 99 percent of the ultimate stress levels, implying that the blade had reached its failure point at the design speed used. Similarly, interlaminar stresses reached 87 percent of an approximate ultimate stress for a matrix. These results indicate that the composite blade would be limited to operation at speeds well below the design value used in the analysis.

In evaluating these results, it must be noted that the weight savings for the composite blade are more than 50 percent when compared to the conventional blade made of metal alone.

SIMPLIFIED STRESS/DEFLECTION CALCULATION FOR A COMPOSITE BLADE

It is usually quite involved and time consuming to predict the detailed stresses and deflections of a composite blade using a 3D finite element method. To expedite the calculation process during the preliminary design phase, it is often desirable and useful for a designer to have a simplified method to quickly estimate the conventional bending and shearing stresses and deflections. In what follows, a simple scheme for predicting stress and deflection is briefly described.

DETERMINATION OF FORCES AND MOMENTS

In a right-handed Cartesian reference frame, the unit base vectors are

$(\underline{i}, \underline{j}, \underline{k})$ for the x-, y-, and z-axes. The x-axis is positive downstream; y-axis is positive starboard; z-axis is positive upward. The hydrodynamic force ($\underline{F}_h$) at each radial cross section is

$$\underline{F}_h = -F_h \cos \phi_p \, \underline{i} + F_h \sin \phi_p \, \underline{e}_\theta$$

where $\underset{\sim}{e}_\theta = -\cos\theta\underset{\sim}{j} - \sin\theta\underset{\sim}{k}$

$\theta = \tan^{-1}(-y/z)$

The centrifugal force $(\underset{\sim}{F}_c)$ at each section is

$\underset{\sim}{F}_c = F_c\underset{\sim}{e}_r ,$

where $\underset{\sim}{e}_r = -\sin\theta\underset{\sim}{j} + \cos\theta\underset{\sim}{k}$.

The corresponding hydrodynamic moment (M_h) and centrifugal moment (M_c) are

$\underset{\sim}{M}_h = \underset{\sim}{d} \times \underset{\sim}{F}_h$

$\underset{\sim}{M}_c = \underset{\sim}{d} \times \underset{\sim}{F}_c$

where $\underset{\sim}{d}$ is the displacement vector between each section.

Assuming that the root section is fixed, the blade acts like a cantilever beam. The moments at each section are determined by integrating the corresponding forces from tip (free) end down to the section of interest.

CALCULATION OF BLADE STRESS

The bending stresses are approximately calculated as follows:

$$\left.\begin{array}{l}\sigma_k \text{ (ps)} \\ \sigma_k \text{ (ss)}\end{array}\right\} = \frac{M_k\left(\pm\frac{t_k}{2}\right)}{I_k} + \frac{F_k}{a_k}$$

where $M_k =$ In-plane moment about the nose-tail line

$t_k =$ Maximum blade cross section thickness

$I_k =$ Moment of inertia about the nose-tail line $\left(\dfrac{(EI)_k}{E_{skin}}\right)$

a_k =   Cross section area occupied by composite skin layer

s_k =   Shell skin layer thickness in the composite blade section

k =   Radial section station index

ps =   pressure side

ss =   suction side

The shear stress is calculated as

$$\tau_k = -\frac{Q_k}{2A_k \, s_k}$$

where Q_k =   Torque in the radial direction

A_k =   Total blade cross section area

Assuming that the root section is fixed, the blade acts like a cantilever beam. The moments at each section are determined by integrating the corresponding forces from tip (free) and down to the section of interest.

CALCULATION OF TIP DEFLECTIONS

In this simplified deflection calculation, only the in-plane moments and the corresponding bending rigidities about the nose-tail line of each section were considered. The bending rigidity of each section was calculated as the product of the effective elastic modulus (following [10]) in the bending axis and the moment of inertia of the cross section about the nose-tail line, for which each section was represented as an elliptical shell having its major axis coincident with the noise-tail line. This approximation introduces inaccuracy because the noise-tail line might not pass through the neutral axis, and the section is not, in general, elliptical. Improved accuracy can be obtained by externally determining the moment of inertia and inserting those values into the computation..

Once the distribution of in-plane moments ($M(x)$) and the bending rigidities ($EI(x)$) are known, the maximum tip deflection is computed as

$$\delta_{tip} = \int_{x=x_{hub}}^{R} \frac{M(x)\,(R-x)}{EI(x)}\, dx \; .$$

To evaluate this simplified method, the stress and deflection of the previously analyzed composite blade were calculated. The program input and resulting output are given in Appendix B, along with a FORTRAN computer code for these calculations.

RESULTS OF SIMPLIFIED CALCULATION

Stress values were calculated at nine stations from the root to the tip, for the mid-chord location. Maximum stresses occurred at the root section. The maximum stress values, which are given in Table 6, ranged from 7 to 50 percent below the finite-element values.

The deflection calculation also showed a lower value with the simplified approach. As shown in Table 6, the calculated tip deflection was 28 percent below the finite element value.

DISCUSSION

ANALYTICAL APPROACHES

The finite-element approach proved suitable for relatively comprehensive analysis of the performance of the composite blade. The treatment level appeared sufficient for use in assessing the adequacy of a particular blade design for at least preliminary design purposes. It is true, however, that not all aspects of the composite structure were represented in the present analysis. Simplifications were made because of the extraordinary complexity of composite structures, and because further work would have required a disproportionate investment of resources.

Composite blade design would benefit from an even simpler structural design approach. However, as illustrated by the present simplified method, further simplification can result in the loss of significant features (such as interlaminar stress) of the structure. A further apparent deficiency of the present approach was its unconservative stress predictions, unlike the beam analysis for a solid, isotropic blade, which gave conservative results. These results show that further exploration is needed of approaches for simplified stress and deflection predictions.

Shell structure performance typically is governed by bending stresses in the outer layer, and by shear stiffness of webs and core. Composite shell analysis must pay attention to through-the-thickness stress as well, because of the relatively weaker strength of the matrix which may predominate in the through-the-thickness direction. This finding suggests that simplified approaches may not be able to be based on two-dimensional stress models.

Even if stress distributions could be determined reliably, application of meaningful failure criteria remains as a problem. A primary deficiency of the present analyses, and perhaps of the field in general, is absence of detailed failure criteria. In composites, failure processes, such as fiber rupture and buckling, fiber/matrix debonding, matrix yielding/cracking, and delamination, can occur in a very complex way. Furthermore, many factors, such as the residual stresses due to fabrication, nonlinear and inelastic effects, and interface interactions between fibers and matrix, do not appear to be properly accounted for in available theory.

As a result of these deficiencies, current approaches to composite material strength and failure are semi-empirical in nature. These approaches must be developed to a sufficient degree to support propeller blade design if such blade structures are to be accepted for vehicular use. Simplified methods, while highly desirable for preliminary design estimates, may be problematical. The large deviations found between the simplified and finite-element methods suggests that a large error allowance would be required if the present simplified method were to be used for preliminary design.

The author would like to emphasize the need for development of fatigue limits for evaluating the feasibility of blades such as the present one. Such limits would presumably include techniques for experimentally certifying candidate structures, such as are used for current metal blades.

COMPOSITE BLADE PERFORMANCE

The present blade example was intended to demonstrate the similarities and differences between conventional NAB and composite thick-shell blade structures. Substitution of a lower-modulus FRP material, with the resulting much-larger stress and deflection values, did not produce an equivalently performing propeller blade. Rather, it provides a frame of reference to assist designers who are just beginning to explore applications of the new material to become familiar with what may be radically different features and parameter values. In this vein, both structural and hydrodynamic designers may need to modify their designs and analysis methods to exploit potential benefits of composite materials.

One such new behavioral characteristic of composite blades may be larger deflections. Acceptability of a large tip deflection, in the present case about 1.7 percent of the overall propeller radius and an order of magnitude greater than that of the NAB blade, must be evaluated in terms of powering performance. No study of the hydrodynamic implications of the deflection was performed.

A second new characteristic is stress levels for which no established interpretation exists. Stress values will require interpretation in terms of established working levels. Even without established levels, of course, the

present stress levels were clearly unacceptable at the speed used. At a minimum, the present composite blade would be limited to speeds well below those at which the NAB blade would reach its working stress.

A third new characteristic is interlaminar stresses. Such stresses may cause failure at levels which would be acceptable for intralaminar stresses. The present example suggests that a critical region for such stresses may be the small-radius aft edge of the blade strength member.

Despite the above differences, there was considerable similarity between the qualitative stress patterns in the plane of the composite shell and parallel to the solid blade surface. In that respect, the composite blade may exhibit relatively "conventional" behavior.

Lastly, a complete feasibility study of a composite blade structure should include variations in material properties such as fiber stiffness and strength as well as blade section geometry, which were not included in the present study.

CONCLUSIONS

1. Three-dimensional finite-element stress analysis appears to be adequate for preliminary design of composite blades.

2. The present composite-adapted beam theory approach for rapidly estimating stresses and deflections in thick-shell composite blades is not adequate for use in preliminary blade design.

3. Establishment of acceptable working stress levels for composite propeller blade structures is required for successful blade design.

4. Use of composite blade structures may be possible in more applications if larger blade deflections than for conventional metal blades can be accepted.

RECOMMENDATIONS

1. A satisfactory method for rapidly estimating blade stresses in preliminary design should be developed.

2. Working stress levels should be determined for composite-material propeller blades.

3. Effects of large blade deflections on blade hydrodynamic performance should be determined.

ACKNOWLEDGMENTS

APPENDIX A.
STIFFNESS MATRIX FOR GENERAL ORTHOTROPIC MATERIALS

For general orthotropic materials, the stiffness matrix is given by the following stress-strain relation :

$$
\begin{Bmatrix} \sigma_1 \\ \sigma_2 \\ \sigma_3 \\ \tau_{12} \\ \tau_{23} \\ \tau_{31} \end{Bmatrix} =
\begin{bmatrix}
c_{11} & c_{12} & c_{13} & 0 & 0 & 0 \\
c_{12} & c_{22} & c_{23} & 0 & 0 & 0 \\
c_{13} & c_{23} & c_{33} & 0 & 0 & 0 \\
0 & 0 & 0 & c_{44} & 0 & 0 \\
0 & 0 & 0 & 0 & c_{55} & 0 \\
0 & 0 & 0 & 0 & 0 & c_{66}
\end{bmatrix}
\begin{Bmatrix} \varepsilon_1 \\ \varepsilon_2 \\ \varepsilon_3 \\ \gamma_{12} \\ \gamma_{23} \\ \gamma_{31} \end{Bmatrix}
$$

where

σ_1, σ_2, σ_3 = normal stresses in the 1, 2, 3 directions ;

τ_{12}, τ_{23}, τ_{31} = shearing stresses in the 1-2, 2-3, and 3-1 planes ;

ε_1, ε_2, ε_3 = normal strains in the 1, 2, 3 directions

γ_{12}, γ_{23}, γ_{31} = shearing strains in the 1-2, 2-3, and 3-1 planes.

Note that there is no interaction between normal stress and shearing strain or shearing stress and normal strain and that there are only nine independent constants in this stiffness matrix.

The stiffness matrix components for a layer of orthotropic material are:

$$ c_{11} = \frac{1 - v_{23} \, v_{32}}{E_2 \, E_3 \, \Delta} $$

$$ c_{12} = \frac{v_{21} + v_{31} \, v_{23}}{E_2 \, E_3 \, \Delta} = \frac{v_{12} + v_{13} \, v_{32}}{E_1 \, E_3 \, \Delta} $$

$$ c_{13} = \frac{v_{31} + v_{21} \, v_{32}}{E_2 \, E_3 \, \Delta} = \frac{v_{13} + v_{12} \, v_{23}}{E_1 \, E_2 \, \Delta} $$

$$C_{22} = \frac{1 - \nu_{13} \nu_{31}}{E_1 E_3 \Delta}$$

$$C_{23} = \frac{\nu_{32} + \nu_{12} \nu_{31}}{E_1 E_3 \Delta} = \frac{\nu_{23} + \nu_{21} \nu_{13}}{E_1 E_2 \Delta}$$

$$C_{33} = \frac{1 - \nu_{12} \nu_{21}}{E_1 E_2 \Delta}$$

$$C_{44} = G_{12}$$

$$C_{55} = G_{23}$$

$$C_{66} = G_{31}$$

E_1, E_2, E_3 = Young's moduli in 1, 2, and 3 directions, respectively

ν_{ij} = Poisson's ratio for transverse strain in the j-direction (ε_j) over the strain (ε_i) by stressing in the i-direction

where

$$\Delta = \frac{1 - \nu_{12} \nu_{21} - \nu_{23} \nu_{32} - \nu_{31} \nu_{13} - 2 \nu_{12} \nu_{32} \nu_{13}}{E_1 E_2 E_3}$$

APPENDIX B.
PROGRAM BSINP — A SIMPLIFIED METHOD OF STRESS AND DEFLECTION CALCULATIONS FOR COMPOSITE BLADES

INPUT FORMAT

The input to BSIMP is read as the following

read 32,title

read *, kd, nxr, dim, rpm, sthk, eskin, eprop

read *, (yr(i), i=nxr,1,-1)

read *, (ph(i), i=nxr,1,-1)

read *, (rake(i), i=nxr,1,-1)

read *, (th(i), i=nxr,1,-1)

read *, (c(i), i=nxr,1,-1)

read *, (t(i), i=nxr,1,-1)

read *, (fdp(i), i=nxr,1,-1)

read *, (wt(i), i=nxr,1,-1)

read *, (sar(i), i=nxr,1,-1)

read *, (seix(i), i=nxr,1,-1)

read *, (peix(i), i=nxr,1,-1)

The variables are defined below.

Card 1: Title

This is a 72-character title for the problem identification.

Card 2: kd, nxr, dim, rpm, sthk, eskin, eprop

kd is an integer variable identifying the the type of units used in the input.

kd =0 indicates that the unit will be of dimensional form;

kd >0 indicates that the unit will be of non-dimensional form;

nxr: Number of input radii;

dim: Thruster diameter;

rpm: Thruster shafter rotational speed in revolution per minute;

sthk: Shell skin-layer thickness in the composite blade section;

eskin: Effective elastic modulus of skin-layer in the bending axis;

eprop: Elastic modulus of solid blade with isotropic material.

Card 3: (yr(i), i=nxr,1,-1)

This card contains nxr values of nondimensional radius

card 4: (ph(i), i=nxr,1,-1)

If kd =0, this card contains nxr values of blade pitch angle in degrees;

If kd >0, this card contains nxr values of pitch-to-diameter ratio.

Card 5: (rake(i), i=nxr,1,-1)

If kd =0, this card contains nxr values of total rake;

If kd >0, this card contains nxr values of total- rake-to-diameter ratio.

Card 6: (th(i), i=nxr,1,-1)

This card contains nxr values of skew angle in degrees.

Card 7: (c(i), i=nxr,1,-1)

If kd =0, this card contains nxr values of chord-length;

If kd >0, this card contains nxr values of chord-to-diameter ratio.

Card 8: (t(i), i=nxr,1,-1)

>   If kd =0, this card contains nxr values of blade section
>   maximum thickness;
>
>   If kd >0, this card contains nxr values of thickness-to-chord
>   ratio.

Card 9: (fdp(i), i=nxr,1,-1)

>   This card contains nxr values of hydrodynamic force per unit
>   length.

Card 10: (wt(i), i=nxr,1,-1)

>   This card contains nxr values of centrifugal force per unit
length.

Card 11: (sar(i), i=nxr,1,-1)

>   This card contains nxr values of cross-sectional area of
>   composite blade.

Card 12: (seix(i), i=nxr,1,-1)

>   This card contains nxr values of effective bending rigidities (=EI)
>   of composite blade section.

Card 13: (peix(i), i=nxr,1,-1)

>   This card contains nxr values of bending rigidities (=EI) of
>   isotropic, solid blade section.

VARIABLE DEFINITIONS

The major outputs are the following variables:

xr: Nondimensional radius.

fip: In-plane force in the nose-tail line (positive toward the trailing
edge).

fop: Out-of-plane force (positive toward suction side).

fri: Force in the radial direction.

mip: In-plane moment about the nose-tail line (positive toward the trailing edge).

mop: Out-of-plane moment (positive toward suction side).

mz: Torque in the radial direction.

smps: Tensile stress at midchord of blade pressure side.

smss: Compressive stress at midchord of blade suction side.

tau: Shearing stress at midchord close to the blade surface.

EXAMPLE INPUT FOR COMPOSITE BLADE

0 9 8.2779 4195.0 0.04 0.285 1.8A

0.231 0.3 0.4 0.5 0.6 0.7 0.8 0.9 1.0

34.833 30.542 30.040 29.417 26.371 22.181 17.344 12.691 8.223

-0.0441 -0.09465 -0.11279 -0.05006 0.07630 0.20929 0.30307 0.34258 0.31316

-3.805 -7.402 -6.750 -2.458 3.551 10.152 16.792 23.399 30.0

1.42225 1.46519 1.51486 1.54202 1.54150 1.49830 1.36689 1.07561 0.57531

0.3038 0.2914 0.2682 0.2384 0.2061 0.1714 0.1358 0.1002 0.0621

0.0000   -3.4010   1.7283   11.0722   20.0709   24.4383   20.5959   5.0384
0.0000

0.755E-02   0.769E-02   0.781E-02   0.780E-02   0.765E-02   0.729E-02
0.653E-02   0.502E-02   0.256E-02

0.103   0.105   0.107   0.107   0.105   0.999E-01   0.894E-01
0.688E-01   0.350E-01

0.348E-03   0.324E-03   0.276E-03   0.211E-03   0.147E-03   0.902E-04
0.449E-04   0.150E-04   0.195E-05

0.353E-02   0.320E-02   0.259E-02   0.185E-02   0.119E-02   0.665E-03
0.304E-03   0.956E-04   0.120E-04

EXAMPLE OUTPUT FOR A COMPOSITE BLADE

kd = 0 (Dimensional input)

kd,ns,dim(in),rpm,sthk(in),eskin(10**7 psi),eprop(10**7 psi) = 0   9   8.278
4195.000   0.040   0.285   1.800

xr   = 0.2310   0.3000   0.4000   0.5000   0.6000   0.7000   0.8000
0.9000   1.000

ph (deg)   = 34.83   30.54   30.04   29.42   26.37   22.18   17.34
12.69   8.223

rake (in)   = -0.4410E-01 -0.9465E-01 -0.1128   -0.5006E-01 0.7630E-01 0.2093
0.3031   0.3426   0.3132

th (deg)   = -3.805   -7.402   -6.750   -2.458   3.551   10.15   16.79
23.40   30.00

c (in)   = 1.422   1.465   1.515   1.542   1.542   1.498   1.367
1.076   0.5753

t (in)   = 0.3038   0.2914   0.2682   0.2384   0.2061   0.1714   0.1358
0.1002   0.6210E-01

fdp (lb/in) = 0.0000   -3.401   1.728   11.07   20.07   24.44   20.60
5.038   0.0000

wt (lb/in)   = 0.7550E-02 0.7690E-02 0.7810E-02 0.7800E-02 0.7650E-02
0.7290E-02 0.6530E-02 0.5020E-02 0.2560E-02

sar (sq.in) = 0.1030   0.1050   0.1070   0.1070   0.1050   0.9990E-01
0.8940E-01 0.6880E-01 0.3500E-01

seix(10**7 psi) = 0.3480E-03 0.3240E-03 0.2760E-03 0.2110E-03 0.1470E-03
0.9020E-04 0.4490E-04 0.1500E-04 0.1950E-05

peix(10**7 psi) = 0.3530E-02 0.3200E-02 0.2590E-02 0.1850E-02 0.1190E-02
0.6650E-03 0.3040E-03 0.9560E-04 0.1200E-04

i	xr	fip	fop	fri	mip	mop	mz
1	1.000	0.000	0.000	0.000	0.000	0.000	0.000
2	0.900	0.123	1.070	3.021	0.064	0.559	-0.117
3	0.800	0.491	6.547	7.088	0.629	2.448	-1.375
4	0.700	0.553	16.267	11.017	4.214	5.654	-5.927
5	0.600	0.302	26.111	14.091	11.362	9.829	-14.332
6	0.500	0.092	33.317	16.199	21.415	13.786	-24.584
7	0.400	0.820	36.610	17.839	33.818	15.456	-32.316
8	0.300	0.683	36.380	19.943	48.121	15.414	-32.976
9	0.231	-3.097	35.085	22.279	58.487	18.958	-26.542

————— ***** Deflection at tips ***** —————

deflection (in.) solid/hollow = 0.5608E-02 0.5159E-01

i	xr	smps	smss	tau
1	0.231	7492.080	-7059.476	1158.489
2	0.300	6357.235	-5977.375	1464.808
3	0.400	4849.579	-4516.136	1528.174
4	0.500	3599.255	-3296.462	1312.994
5	0.600	2404.279	-2135.874	914.579
6	0.700	1251.428	-1030.875	492.272
7	0.800	350.336	-191.765	172.170
8	0.900	-17.326	105.136	29.749
9	1.000	0.000	0.000	0.000

Fortran STOP

```
      program bsimp
      implicit real*8 (a-h,o-z)
      parameter (nx=15)
      character*72,title
      dimension x(nx),y(nx),z(nx),th(nx),rake(nx),rx(nx),ph(nx),sm(nx),
     1 c(nx),wt(nx),fdp(nx),cf(nx),cfy(nx),cfz(nx),fip(nx),fop(nx),
     2 fr(nx),bmip(nx),bmop(nx),tmz(nx),bmih(nx),bmoh(nx),tmh(nx),
     3 bmic(nx),bmoc(nx),tmc(nx),xr(nx),bm1(nx),bm2(nx),seix(nx),
     4 peix(nx),sei(nx),pei(nx),smei(nx),pmei(nx),yr(nx),six(nx),pix(nx)
      dimension tmq(nx),cfr(nx),ch(nx),t(nx),tk(nx),sar(nx),sa(nx),
     1 sigps(nx),sigss(nx),tau(nx)
c--- kd =0 (dim lb-in unit), kd >0 (nondim unit:p/d,it/d,c/d,t/c,f/c)
      pi=3.141592654
      rd=pi/180.0
      j1=1
      read 32,title
      read *,kd,nxr,dim,rpm,sthk,eskin,eprop
      read *,(yr(i),i=nxr,1,-1)
      read *,(ph(i),i=nxr,1,-1)
      read *,(rake(i),i=nxr,1,-1)
      read *,(th(i),i=nxr,1,-1)
      read *,(c(i),i=nxr,1,-1)
      read *,(t(i),i=nxr,1,-1)
      read *,(fdp(i),i=nxr,1,-1)
      read *,(wt(i),i=nxr,1,-1)
      read *,(sar(i),i=nxr,1,-1)
      read *,(seix(i),i=nxr,1,-1)
      read *,(peix(i),i=nxr,1,-1)
      print 30,' --- output of ',title
      if (kd .eq. 0) print 31,'kd = ',kd,' ( Dimensional input )'
      if (kd .ne. 0) print 31,'kd = ',kd,' ( Nondimensional input )'
      if (kd .eq. 0) go to 10
      do 11 i=1,nxr
      ph(i)=datan(ph(i)/yr(i)/pi)/rd
      rake(i)=rake(i)*dim
      c(i)=c(i)*dim
      t(i)=t(i)*c(i)
   11 continue
   10 continue
      print 24,'kd,ns,dim(in),rpm,sthk(in),eskin(10**7 psi),eprop(10**7
     1psi) =',kd,nxr,dim,rpm,sthk,eskin,eprop
      print 23,'xr          =',(yr(i),i=nxr,1,-1)
      print 23,'ph (deg)    =',(ph(i),i=nxr,1,-1)
      print 23,'rake (in)   =',(rake(i),i=nxr,1,-1)
      print 23,'th (deg)    =',(th(i),i=nxr,1,-1)
```

```
print 23,'c (in)      =',(c(i),i=nxr,1,-1)
print 23,'t (in)      =',(t(i),i=nxr,1,-1)
print 23,'fdp (lb/in)  =',(fdp(i),i=nxr,1,-1)
print 23,'wt  (lb/in)  =',(wt(i),i=nxr,1,-1)
print 23,'sar (sq.in)  =',(sar(i),i=nxr,1,-1)
print 23,'seix(10**7 psi) =',(seix(i),i=nxr,1,-1)
print 23,'peix(10**7 psi) =',(peix(i),i=nxr,1,-1)
rad=0.5*dim
rad2=rad*rad
print 26
romga=rpm*pi/30.0
fop(1)=0.0
fip(1)=0.0
bmip(1)=0.0
bmop(1)=0.0
tmz(1)=0.0
fxi=0.0
fyi=0.0
fzi=0.0
bmx=0.0
bmy=0.0
bmz=0.0
bmip(1)=0.
bmop(1)=0.
tmz(1)=0.0
fxhi=0.0
fyhi=0.0
fzhi=0.0
fyci=0.0
fzci=0.0
bhx=0.0
bhy=0.0
bhz=0.0
bcx=0.0
bcy=0.0
bcz=0.0
rx(1)=yr(1)*rad
do 1 i=2,nxr
rx(i)=yr(i)*rad
ths=th(i)*rd
thsm1=th(i-1)*rd
x(i)=rake(i)
x(i-1)=rake(i-1)
sth=dsin(ths)
cth=dcos(ths)
sthm1=dsin(thsm1)
cthm1=dcos(thsm1)
```

```
y(i)=-rx(i)*sth
z(i)= rx(i)*cth
y(i-1)=-rx(i-1)*sthm1
z(i-1)= rx(i-1)*cthm1
dx=x(i-1)-x(i)
dy=y(i-1)-y(i)
dz=z(i-1)-z(i)
dr=rx(i-1)-rx(i)
adr=dabs(dr)
sm(i)=wt(i)/32.2
cf(i)=sm(i)*(rx(i)/12.0)*romga*romga
cfy(i)=-cf(i)*sth
cfz(i)= cf(i)*cth
sm(i-1)=wt(i-1)/32.2
cf(i-1)=sm(i-1)*(rx(i-1)/12.0)*romga*romga
cfy(i-1)=-cf(i-1)*sthm1
cfz(i-1)= cf(i-1)*cthm1
phi=ph(i)*rd
sphi=dsin(phi)
cphi=dcos(phi)
phim1=ph(i-1)*rd
sphim1=dsin(phim1)
cphim1=dcos(phim1)
cpct=cphi*cth
cpst=cphi*sth
spct=sphi*cth
spst=sphi*sth
cpctm1=cphim1*cthm1
cpstm1=cphim1*sthm1
spctm1=sphim1*cthm1
spstm1=sphim1*sthm1
fhxu=-0.5*fdp(i-1)*cphim1*adr
fhxb=-0.5*fdp(i)*cphi*adr
fhyu=-0.5*fdp(i-1)*spctm1*adr
fhyb=-0.5*fdp(i)*spct*adr
fhzu=-0.5*fdp(i-1)*spstm1*adr
fhzb=-0.5*fdp(i)*spst*adr
fcyu=0.5*cfy(i-1)*adr
fcyb=0.5*cfy(i)*adr
fczu=0.5*cfz(i-1)*adr
fczb=0.5*cfz(i)*adr
fhxi=fhxu+fhxb
fhyi=fhyu+fhyb
fhzi=fhzu+fhzb
fcyi=fcyu+fcyb
fczi=fczu+fczb
fxim1=fxi
```

```
fyim1=fyi
fzim1=fzi
fxhim1=fxhi
fyhim1=fyhi
fzhim1=fzhi
fycim1=fyci
fzcim1=fzci
fxhi=fxhi+fhxi
fyhi=fyhi+fhyi
fzhi=fzhi+fhzi
fyci=fyci+fcyi
fzci=fzci+fczi
fxi=fxi+fhxi
fyi=fyi+fhyi+fcyi
fzi=fzi+fhzi+fczi
fip(i)=fxi*sphi-fyi*cpct-fzi*cpst
fop(i)=-fxi*cphi-fyi*spct-fzi*spst
fr(i)=-fyi*sth+fzi*cth
bmhx=(0.75*fhzu+0.25*fhzb)*dy-(0.75*fhyu+0.25*fhyb)*dz
bmhy=(0.75*fhxu+0.25*fhxb)*dz-(0.75*fhzu+0.25*fhzb)*dx
bmhz=(0.75*fhyu+0.25*fhyb)*dx-(0.75*fhxu+0.25*fhxb)*dy
bmcx=(0.75*fczu+0.25*fczb)*dy-(0.75*fcyu+0.25*fcyb)*dz
bmcy=-(0.75*fczu+0.25*fczb)*dx
bmcz= (0.75*fcyu+0.25*fcyb)*dx
if (i .ne. 2 ) go to 3
bmx=bmx+bmhx+bmcx
bmy=bmy+bmhy+bmcy
bmz=bmz+bmhz+bmcz
bhx=bhx+bmhx
bhy=bhy+bmhy
bhz=bhz+bmhz
bcx=bcx+bmcx
bcy=bcy+bmcy
bcz=bcz+bmcz
go to 4
3 bmx=bmx+bmhx+bmcx+fzim1*dy-fyim1*dz
bmy=bmy+bmhy+bmcy+fxim1*dz-fzim1*dx
bmz=bmz+bmhz+bmcz+fyim1*dx-fxim1*dy
bhx=bhx+bmhx+fzhim1*dy-fyhim1*dz
bhy=bhy+bmhy+fxhim1*dz-fzhim1*dx
bhz=bhz+bmhz+fyhim1*dx-fxhim1*dy
bcx=bcx+bmcx+fzcim1*dy-fycim1*dz
bcy=bcy+bmcy-fzcim1*dx
bcz=bcz+bmcz+fycim1*dx
4 bmip(i)=bmx*sphi-bmy*cpct-bmz*cpst
bmop(i)=-bmx*cphi-bmy*spct-bmz*spst
tmz(i)=-bmy*sth+bmz*cth
```

```fortran
      bmih(i)=bhx*sphi-bhy*cpct-bhz*cpst
      bmoh(i)=-bhx*cphi-bhy*spct-bhz*spst
      tmh(i)=-bhy*sth+bhz*cth
      bmic(i)=bcx*sphi-bcy*cpct-bcz*cpst
      bmoc(i)=-bcx*cphi-bcy*spct-bcz*spst
      tmc(i)=-bcy*sth+bcz*cth
    1 continue
c     print 25
c     do 5 i=2,nxr
c     print 21,i,bmih(i),bmoh(i),tmh(i),bmic(i),bmoc(i),tmc(i)
c   5 continue
      print 20
      do 2 i=1,nxr
      print 21,i,yr(i),fip(i),fop(i),fr(i),bmip(i),bmop(i),tmz(i)
    2 continue
      bmip(1)=0.0
      do 7 i=1,nxr
      ii=nxr-i+1
      xr(i)=yr(ii)
      bm1(i)=bmip(ii)
      tmq(i)=tmz(ii)
      cfr(i)=fr(ii)
      ch(i)=c(ii)
      tk(i)=t(ii)
      sa(i)=sar(ii)
      six(i)=seix(ii)/eskin
      pix(i)=peix(ii)/eprop
      sei(i)=seix(ii)*10.0**7
      pei(i)=peix(ii)*10.0**7
    7 continue
      print 26
c     print 23,' xr =',(xr(i),i=1,nxr)
c     print 23,' bm =',(bm1(i),i=1,nxr)
c     print 23,' seix =',(seix(i),i=nxr,1,-1)
c     print 23,' peix =',(peix(i),i=nxr,1,-1)
c     print 23,' sei =',(sei(i),i=1,nxr)
c     print 23,' pei =',(pei(i),i=1,nxr)
      do 6 i=1,nxr
      xr1=1.0-xr(i)
      smei(i)=bm1(i)*xr1/sei(i)
      pmei(i)=bm1(i)*xr1/pei(i)
c     print 19,i,xr1,bm1(i),sei(i),smei(i),pmei(i)
    6 continue
c     print 23,' smei =',(smei(i),i=1,nxr)
c     print 23,' pmei =',(pmei(i),i=1,nxr)
      print 27
      defc=1.0*rad2*simpun(xr(1),smei(1),nxr)
```

```fortran
      defp=1.0*rad2*simpun(xr(1),pmei(1),nxr)
      print 23,' deflection (in.) solid/hollow = ',defp,defc
      print 26
      do 8 i=1,nxr
      ty=0.5*tk(i)
      ax=0.5*(ch(i)-sthk)
      by=ty-0.5*sthk
      az=pi*ax*by
      yps=ty
      yss=-ty
      sigps(i)=bm1(i)*yps/six(i)+cfr(i)/sa(i)
      sigss(i)=bm1(i)*yss/six(i)+cfr(i)/sa(i)
      tau(i)=-0.5*tmq(i)/(az*sthk)
    8 continue
      print 29
      do 9 i=1,nxr
      print 21,i,xr(i),sigps(i),sigss(i),tau(i)
    9 continue
   19 format (i3,12(g9.2,1x))
   20 format (/' i      xr       fip       fop       fri
     1     mip        mop       mz ')
   21 format (i3,7(f12.3,2x))
   22 format (2i3,12(f10.3,1x))
   23 format (a,10(g12.4,1x))
   24 format (a,2i4,2x,10(f8.3,1x))
   25 format (/' i     bmih       bmoh       tmh       bmi
     1c     bmoc      tmc ')
   26 format ('----------------------------------------')
   27 format (/' -------- ***** Deflection at tips ***** --------'/)
   28 format (/)
   29 format (' i     xr       smps      smss      tau ')
   30 format (/a,a/)
   31 format (a,i3,2x,a)
   32 format (a)
      stop
      end
      FUNCTION SIMPUN( X, Y, N )
      IMPLICIT REAL*8 (A-H,O-Z)
C
C     FORTRAN IV FUNCTION FOR SIMPSON'S RULE INTEGRATION
C         ARBITRARY NO. AND LENGTH INTERVALS
C
      DIMENSION X(15), Y(15)
C
      IF ( N .LE. 1 ) THEN
C
C         N .LE. 1 -- *****ERROR*****
C
```

```fortran
C          RETURN ZERO ANSWER
C
      SIMPUN = 0.0
      ELSE IF ( N .EQ. 2 ) THEN
C
C        N = 2 -- USE TRAPAZOIDAL RULE
C
      SIMPUN = (Y(1) + Y(2))*(X(2) - X(1))/2.0
      ELSE
C
C        N .GE. 3 -- USE SIMPSON'S RULE
C
      IF ( MOD( N, 2 ) .EQ. 0 ) THEN
C
C          N IS EVEN, TAKE A SPECIAL STEP TO START THE INTEGRATION
C
      DX21 = X(2) - X(1)
      DX31 = X(3) - X(1)
      DX32 = X(3) - X(2)
      S = DX21*( Y(1)*(3.0 - DX21/DX31) +
     1           Y(2)*(3.0 + DX21/DX32) -
     2           Y(3)*DX21**2/(DX31*DX32) )/6.0
      L = 3
      ELSE
C
C          N IS ODD, NOTHING SPECIAL REQUIRED
C
      S = 0.0
      L = 2
      END IF
      DO 1000 K = L, N-1, 2
      ABSDX = dABS( X(K) - X(1) )
      IF ( dABS( X(K-1) - X(1) ) .GE. ABSDX .OR.
     1      ABSDX .GE. dABS( X(K+1) - X(1) ) ) GO TO 1100
      DXKPKM = X(K+1) - X(K-1)
      DXKKM = X(K) - X(K-1)
      DXKPK = X(K+1) - X(K)
      S = S + DXKPKM*( Y(K-1)*(3.0 - DXKPKM/DXKKM) +
     1            Y(K)*(1.0 + DXKPKM/DXKKM + DXKKM/DXKPK) +
     2            Y(K+1)*(2.0 - DXKKM/DXKPK) )/6.0
1000  CONTINUE
      SIMPUN = S
      END IF
      GO TO 99999
1100  CONTINUE
      print 100, K, X(K)
      SIMPUN = 0.0
99999 CONTINUE
      RETURN
100   FORMAT(23H0NON MONOTONE X SIMPUN   , I4, 1PE12.4)
      END
```

REFERENCES

1. Jones, R.M., "Mechanics of Composite Materials," Scripta Book Company, Washington, D.C. (1975).

2. Hashin, Z., "Analysis of Composite Materials—a Survey," Journal of Applied Mechanics, Vol.50 (Sep 1983).

3. Lubin, G., "Handbook of Composite," Van Nostrand Reinhold Company (1982).

4. Lin, G.–F., "Three-Dimensional Stress Analysis of a Fiber-Reinforced Composite Thruster Blade," Proceedings of SNAME Propellers/Shafting '91, Virginia Beach, Virginia (Sep 1991).

5. Chamis, C.C. "Simplified Composite Micromechanics Equations for Hygral, Thermal, and Mechanical Properties," SAMPE Quarterly (Apr 1984).

6. Nguyen, L.B. and M.O. Critchfield, "Determination of Laminate Elastic Properties for the Design and Analysis of Fibrous Composite Ship Structure" David Taylor Research Center Report SD-35 (May 1985).

7. Vinson, J .R. and T-W Chou, "Composite Materials and Their Use in Structures," John Wiley & Sons (1975).

8. Whitney, J.M., "Shear Correction Factors for Orthotropic Laminates Under Static Load," Journal of Applied Mechanics (Mar 1973).

9. Pagano, N.J. and R.B. Pipes, "Some Observations on the Interlaminar Strength of Composite Materials," Int. J. Mech. Sci.,Vol 15 (1973).

10. Sun, C.T. and S. Li, "Three-Dimensional Effective Elastic Constants for Thick Laminates," Journal of Composite Materials, Vol 22 (Jul 1988).

11. Scardino, F., "An Introduction to Textile Structures and their Behavior," Chapter 10, 'Textile Structural Composites,' edited by T-W Chou and F.K. Ko (1989).

12. Ko, F.K, "Tensile Strength and Modulus of a Three-Dimensional Braid Composite," Composite Materials: Testing and Design (Seventh Conference) Philadelphia, Pa. (Apr 1984).

13. Ma, C-L, J.M. Yang, and T-W Chou, "Elastic Stiffness of Three-Dimensional Braided Textile Structural Composites," Composite Materials : Testing and Design (Seventh Conference) Philadelphia, Pa. (Apr 1984).

14. Yang, J-M, C-L Ma, and T-W Chou, "Fiber Inclination Model of Three-Dimensional Textile Structural Composites," Journal of Composite Material, Vol 20 (Sep 1986).

15. Ko, F.K., "Three-dimensional Fabrics for Composites," Chapter 5 of "Textile Structural Composites" edited by T-W Chou and F.K. Ko (1989).

16. Whyte, D.W. "On the Structure and Properties of 3-D Braid Reinforced Composites," Ph.D Thesis, Drexel University (Jun 1986).

17. Dobyns, A.L. et al., "Assessment of the Applicability of Fiber-Reinforced Plastic (FRP) Analysis Methods to Naval Ships Structures, " DTNSRDC Report 85/085 (Sep 1985).

18. Macander, A.B., R.M. Crane, and E.T. Camponeschi,Jr., "Fabrication and Mechanical Properties of Multidimensionally (X-D) Braided Composite Materials, "Composite Materials : Testing and Design (Seventh Conference) Philadelphia, Pa. (Apr 1984).

19. Pagano , N.J, and S.R. Soni, "Global-Local Laminate Variational Model," It. J. Solids Structures, Vol 19, No.3 (1983).

20. Sun, C.T. and Mao, K.M., "A Global-Local Finite Element Method Suitable for Parallel Computations," Computers and Science, Vol 29, No. 2 (1988).

21. Tsai, S.W. and E.M. Wu, "A General Theory of strength for Anisotropic Material," J. Composite Materials 5 (1971).

22. Tsai, S.W., "Introduction to Composite Materials," Technomic Publishing Co. Inc. (1980).

23. Daoust, J. and S.V. Hoa, "A Comprehensive Technique for Determination of Safety Factors in Composites," Journal of Reinforced Plastics and Composites, Vol 8 (Nov 1989).

24. Kruesi, A.H. and D.C. Kruesi, "Preparing to Manufacture 4-Axis Computer Controlled Braided Composite Structures," Conference: The Design, Manufacture, and Quality Assurance of Low Cost, Lightweight Advanced Composite Molds, Tools, and Structures (Oct 1988).

25. Anon., "ABAQUS User's Manual, Version 4.8) " Hibbit, Karlsson & Sorensen, Inc. (1989).

26. Bisshopp R. E. and D. C. Drucker, "Large Deflection of Cantilever Beams", Quarterly of Applied Mathematics, Vol. III, No. 1 (1945).

27. Spilker, R. L., S. Verbiese, O. Orringer, S. E. French, E. A. Witmer, and A. Harris, "Use of the Hybrid-Stress Finite-Element Model for the Static and Dynamic Analysis of Multilayer Composite Plates and Shells," Report for the Army Materials and Mechanics Research Center, Watertown, Mass (1976).

28. Sun C. T. and W. C. Liao, "Analysis of Thick Section Composite Laminates Using Effective Moduli," Journal of Composite Materials, Vol. 24 (Sep 1990).

29. Comstock, J. P. (ed.), "Principles of Naval Architecture," Society of Naval Architects and Marine Engineers, New York (1967).

INITIAL DISTRIBUTION

Copies		Code	Name
3	CNO		
1		222	
1		22T	
1		23B	
2	ONT		
1		23	A.J. Falstich
1		233	G. Remmers
1	OAT	30	J. DeCorpo
1	ONR	113	
13	NAVSEA		
1		501	
1		5027	
1		5112	
1		08	
1		92R	
1		PMS 330	M. Finnerty
1		PMS 350	
1		PMS 393	
1		55N2	
1		55W3	
2		56X7	
1		56XN	
1	NRL	1006	
1	NOSC	634	T. Mautner
1	NUSC	01V	
2	DTIC		
1	ARL/PSU		M. Billet

CENTER DISTRIBUTION

Copies	Code	Name
1	011	H. Chaplin
1	0113	D. Winegrad
1	0114	L. Becker
1	0115	I. Caplan
1	1284	M. Hurwitz
1	1501	D. Goldstein
1	1501	J. Gorski
1	1501	H. Haussling
10	1504	
1	1506	D. Walden
1	1508	J. Brown
1	1509	
1	152	W.-C. Lin
1	1521	W. Day
1	1522	M. Wilson
1	154	J. McCarthy
1	1542	F. Noblesse
1	1543	D. Coakley
1	1544	F. Peterson
1	1544	P. Besch
1	1544	B. Chen
1	1544	C. Dai
1	1544	S. Neely
1	1544	K.-H. Kim
10	1544	G.-F. Lin
1	1702	J. Corrado
1	172	R. Rockwell
1	1720.1	T. Tinley
1	1720.2	D. Bonanni
1	1720.2	S. Mayes
1	1720.2	P. Young

CENTER DISTRIBUTION (Continued)

Copies	Code	Name
1	1944	T. Mathews
1	1944	R. Szwerc
1	1944	J. Gershfeld
1	1944	J. Gonzales
1	2844	P. Coffin
1	2844	D. Loup